

---

Electronic Thesis and Dissertation Repository

---

6-26-2020 1:30 PM

## Metal Additive Manufacturing for Fixed Dental Prostheses

Mai EL Najjar, *The University of Western Ontario*

Supervisor: Rizkalla, Amin, *The University of Western Ontario*

Co-Supervisor: Hosein, Yara, *The University of Western Ontario*

A thesis submitted in partial fulfillment of the requirements for the Master of Engineering  
Science degree in Biomedical Engineering

© Mai EL Najjar 2020

Follow this and additional works at: <https://ir.lib.uwo.ca/etd>



Part of the [Biomaterials Commons](#), [Dental Materials Commons](#), and the [Prosthodontics and Prosthodontology Commons](#)

---

### Recommended Citation

EL Najjar, Mai, "Metal Additive Manufacturing for Fixed Dental Prostheses" (2020). *Electronic Thesis and Dissertation Repository*. 7123.

<https://ir.lib.uwo.ca/etd/7123>

This Dissertation/Thesis is brought to you for free and open access by Scholarship@Western. It has been accepted for inclusion in Electronic Thesis and Dissertation Repository by an authorized administrator of Scholarship@Western. For more information, please contact [wlsadmin@uwo.ca](mailto:wlsadmin@uwo.ca).

## Abstract

The use of additive manufacturing (AM) in dentistry has gained momentum in recent years. However, high initial costs and uncertainty surrounding the quality of AM products are considered barriers to their use. This research compared dental substructures fabricated by AM versus conventional casting and milling.

Cobalt-chromium alloy rectangular bars and three-unit bridge substructures were fabricated by AM, casting or milling. Bars manufactured by AM exhibited superior flexural strength, shear bond strength of porcelain coating, and Vickers hardness. Bridge substructures fabricated by AM showed similar flexural stiffness to cast, similar flexural loads at failure to milled and cast, and overall accuracy of fabrication within 12 micrometers. AM substructures showed exhibited pores primarily within the abutment region comparable to the milled and cast substructures.

Overall, bars and three-unit bridges manufactured by AM exhibited equal or better mechanical properties than those fabricated by conventional techniques.

## Summary for Lay Audience

Additive manufacturing (AM) is a computerized process of depositing materials layer by layer to produce three dimensional objects. The use of AM in dentistry has gained momentum over the last 30 years, with computer-aided design and manufacturing (CAD/CAM) being used for production of dental restorations. Despite the potential benefits of AM, dental labs are hesitant to adopt its use due to high costs for initial production, as well as uncertainty about the quality of the AM products compared to those fabricated using conventional methods. The objective of this research was to compare dental restorations made by AM versus the conventional methods of casting and milling.

Metal (cobalt-chromium) alloy bar samples and three-unit bridge substructures were fabricated by AM and conventional casting and milling methods. Bar samples were designed to conform to testing standards, and geometrically uniform three-unit bridge substructures were custom designed for standardized testing. 3D X-ray images were obtained for a subset of the three-unit-bridge substructures before testing. Bar samples were mechanically tested to assess bending, hardness, and porcelain coating properties. Three-unit bridge substructures were mechanically tested to compare the bending properties of clinically relevant geometries. As well, X-ray images of fabricated three-unit bridges were used to generate 3D models for investigation of internal porosity and surface geometry related to the accuracy of fabrication.

Bar samples manufactured by AM exhibited superior bending strength, hardness, and porcelain coating bond strength compared to cast or milled samples. Three-unit bridges fabricated by AM and casting showed superior bending stiffness compared to milling, while

no differences were found in bending loads at failure among milled, cast, and AM samples. Accuracy of fabrication for three-unit bridges were all within 12 micrometers from the ideal model, with no significant difference among the three groups.

Overall, alloy bar samples and three-unit bridges fabricated by AM showed equivalent or superior performance to those produced by milling or casting. Results from this thesis provide information to the dental manufacturing industry regarding the mechanical performance, internal structure, and accuracy of fabrication of dental restorations manufactured by AM compared to the conventional methods of milling and casting.

## Keywords

Selective laser melting (SLM), Lost-wax casting, Cobalt chromium (Co-Cr), Additive manufacturing (AM), Shear bond strength, Bending strength, Cast, Milled, Computer-aided design (CAD), Computer-aided manufacturing (CAM), 3D printing, Dental manufacturing, Three-unit bridges, Porcelain-fused to metal, Micro-CT imaging

## Co-Authorship Statement

Chapter 1 “Introduction” - Written by Dr. Mai EL Najjar and reviewed by Dr. Amin Rizkalla and Dr. Yara Hosein.

Chapter 2 “Materials and Methods” - All experiments were designed by Dr. Amin Rizkalla, Dr. Yara Hosein and Dr. Mai EL Najjar. Dr. Mai EL Najjar performed experiments and analyses for three-point bending, hardness and shear bond strength tests. Micro-CT imaging and analysis were performed by Dr. Mai EL Najjar, with the assistance of Dr. Andrew Nelson. The chapter was written by Dr. Mai EL Najjar and reviewed by Dr. Amin Rizkalla and Dr. Yara Hosein.

Chapter 3 “Results” - Written by Dr. Mai EL Najjar and reviewed by Dr. Amin Rizkalla and Dr. Yara Hosein.

Chapter 4 “Discussion” - Written by Dr. Mai EL Najjar and reviewed by Dr. Amin Rizkalla and Dr. Yara Hosein.

## Acknowledgments

They say, "Dedication is not what others expect of you, it is what you can give to others, and I know very well that no matter what I give, there are people in my life who I will never be able to give them enough".

To those who paved the way and gave me the enthusiasm, encouragement and helped me through difficult times of my study. To those who allowed me to become a dentist and whose encouragement and sacrifice helped to make it all possible. This work is a small gift from me to all of you, and it is just the first step, it is just a clue to learn how to do research, to know what to do.

I would like to express my special gratitude and thank my supervisor Dr. Amin Rizkalla, for imparting his immense knowledge and expertise in the study.

Special thanks and gratitude to my advisor Dr. Yara Hosein, for the continued support to complete my MEdSc study and research, for her patience, motivation, and enthusiasm.

Without guidance and help from Drs. Rizkalla and Hosein, I could not have imagined having better advisors and mentors during my MEdSc study.

My sincere thanks to my parents, sister and brothers.

Moreover, all other thanks are to my advisory committee Dr. Robert Klassen and Dr. Matt Teeter for their encouragement. They generously contributed their time and effort to help me make this thesis as accurate and useful as possible. Special thanks to Dr. S. Jeffrey Dixon for his support and feedback during my journey of writing my thesis.

Warm thanks to Rotsaert Dental Laboratory (Hamilton, ON) and the Ontario Centres of Excellence - Voucher for Innovation and Productivity (OCE-VIP) program for their

contribution to this research. Many thanks to Dr. Santiago Cobos for his knowledge and expertise in the field of imaging, and many thanks to Dr. David Holdsworth for the use of his research lab and equipment to complete the imaging analysis. Thanks to Dr. Andrew Nelson, for his support in this study. Thanks to Dr. Timothy Burkhart, for his help in this study. Warm thanks to Dan Sweiger from the Machine shop for his assistance. Thanks to all my friends and colleagues for their support.

# Table of Contents

|  |      |
|--|------|
| Abstract .....                                   | i    |
| Summary for Lay Audience .....                   | ii   |
| Keywords .....                                   | iii  |
| Co-Authorship Statement.....                     | iiiv |
| Acknowledgments.....                             | v    |
| Table of Contents .....                          | vii  |
| List of Abbreviations .....                      | xi   |
| List of Tables .....                             | xiii |
| List of Figures .....                            | xiv  |
| List of Appendices .....                         | xvi  |
| Chapter 1 .....                                  | 1    |
| 1 Literature Review and Background .....         | 1    |
| 1.1 Overview.....                                | 1    |
| 1.2 Additive Manufacturing (AM).....             | 2    |
| 1.2.1 Definition of Additive Manufacturing ..... | 2    |



|           |  |    |
|-----------|--|----|
| 1.2.2     | Additive Manufacturing/3D Printing Process.....                | 2  |
| 1.3       | Dental Prosthesis Substructures .....                          | 7  |
| 1.3.1     | Types of Dental Prosthesis.....                                | 7  |
| 1.3.2     | Porcelain Fused to Metal (PFM) Restoration .....               | 12 |
| 1.3.3     | Fabrication of Dental Prosthesis Substructures .....           | 16 |
| 1.3.4     | CAD/CAM Milling Technology.....                                | 21 |
| 1.3.5     | Metal Additive Manufacturing.....                              | 24 |
| 1.4       | Micro Computed Tomography ( $\mu$ -CT) .....                   | 33 |
| 1.4.1     | What is the Micro-CT? .....                                    | 33 |
| 1.5       | Study Rationale.....   | 36 |
| 1.6       | Objective and Hypothesis .....                                 | 37 |
| 1.7       | Thesis Organization .....                                      | 38 |
| Chapter 2 | .....  | 40 |
| 2         | Materials and Methods .....                                    | 40 |
| 2.1       | Materials .....  | 40 |
| 2.1.1     | Cobalt Chromium (Co-Cr) Samples Design and Specification ..... | 40 |
| 2.2       | Methods.....   | 42 |

|           |  |    |
|-----------|--|----|
| 2.2.1     | Fabrication of Rectangular Bars and Three-Unit Bridges Substructures.. | 42 |
| 2.2.2     | Imaging Analysis of Three-Unit Bridges.....                            | 44 |
| 2.2.3     | Mechanical Testing.....  | 46 |
| 2.2.4     | Geometric Accuracy of Fabrication.....                                 | 54 |
| 2.2.5     | Internal Porosity Analysis.....  | 57 |
| 2.2.6     | Analysis of Sectioned Surfaces of Co-Cr alloys.....                    | 60 |
| 2.2.7     | Statistical Analysis.....  | 60 |
| Chapter 3 | .....  | 62 |
| 3         | Results.....   | 62 |
| 3.1       | Overview.....  | 62 |
| 3.2       | Mechanical properties of the Rectangular Bar Specimens .....           | 62 |
| 3.2.1     | Three Point Bend Test for Rectangular Bar Specimens .....              | 62 |
| 3.2.2     | Vickers Hardness for Bar Samples .....                                 | 63 |
| 3.2.3     | Shear Bond Strength for Bar Samples .....                              | 63 |
| 3.3       | Mechanical Properties of Three-Unit Bridges .....                      | 67 |
| 3.3.1     | Three Point Bend Test for Three-Unit Bridge samples .....              | 67 |
| 3.4       | Internal Porosity Analysis.....  | 67 |

|  |     |
|--|-----|
| 3.4.1 Porosity Analysis from Micro-CT imaging .....        | 67  |
| 3.4.2 Porosity Analysis from Metallurgy Investigation..... | 70  |
| 3.5 Geometric Accuracy of Fabrication.....                 | 70  |
| Chapter 4 .....  | 74  |
| 4 Discussion .....   | 74  |
| 4.1 Discussion .....                                       | 74  |
| 4.2 Conclusion .....                                       | 79  |
| References.....  | 81  |
| Appendices.....  | 90  |
| Appendix A.....  | 90  |
| Appendix B.....  | 99  |
| Appendix C.....  | 103 |
| Appendix D.....  | 107 |
| Appendix E.....  | 113 |
| Curriculum Vitae .....                                     | 115 |

## List of Abbreviations

|  |         |
|--|---------|
| Additive Manufacturing                                 | AM      |
| Aluminum   | Al      |
| American Society for Testing and Materials             | ASTM    |
| Boron  | B       |
| Cobalt chromium  | Co-Cr   |
| Computed Tomography                                    | CT      |
| Computer Aided Design and Computer Aided Manufacturing | CAD/CAM |
| Degrees Celsius  | °C      |
| Fixed Partial Denture                                  | FPD     |
| Gallium  | Ga      |
| Iron   | Fe      |
| Kilovoltage  | kV      |
| Micro Ampere   | μA      |
| Micro-CT   | μ-CT    |
| Micrometer   | μm      |

|                           |     |
|---------------------------|-----|
| Millimeter                | mm  |
| Molybdenum                | Mo  |
| Niobium                   | Nb  |
| Porcelain fused to metal  | PFM |
| Pounds per square inch    | psi |
| Rapid Prototyping         | RP  |
| Region of Interest        | ROI |
| Removable Partial Denture | RPD |
| Ruthenium                 | Ru  |
| Selective Laser Melting   | SLM |
| Stereolithography         | STL |
| Three-dimensional         | 3D  |
| Titanium                  | Ti  |
| Tungsten                  | W   |
| Two Dimensional           | 2D  |

## List of Tables

Table 1: Chemical Composition of Co-Cr alloys for AM, Milling and Casting.....43

## List of Figures

|  |    |
|--|----|
| Figure 1-1: Process flow for AM techniques.....  | 6  |
| Figure 1-2: Single Crown.....  | 8  |
| Figure 1-3: Three-Unit Bridge .....  | 10 |
| Figure 1-4: Components of the Three-Unit Bridge FPD .....                                | 11 |
| Figure 1-5: Porcelain-Fused to Metal (PFM) Restorations.....                             | 15 |
| Figure 1-6: Lost Wax techniques (Dental Casting) .....                                   | 17 |
| Figure 1-7: CAD/CAM Milling techniques.....  | 22 |
| Figure 1-8: Workflow of the Selective Laser Melting Process (SLM).....                   | 27 |
| Figure 1-9: Nikon (Micro-CT Scanner XTH 225 ST model).....                               | 35 |
| Figure 2-1: Co-Cr Samples Design.....  | 41 |
| Figure 2-2: Nikon (Micro-CT Scanner XTH 225 ST model).....                               | 45 |
| Figure 2-3:Workflow chart for the full Micro-CT process .....                            | 47 |
| Figure 2-4: Three-point bend test setup for the Rectangular Co-Cr samples.. ..           | 48 |
| Figure 2-5: Three-point bending test set up for the three-unit bridge Co-Cr sample ..... | 50 |
| Figure 2-6: Co-Cr Square sample .....  | 51 |

|   |    |
|---|----|
| Figure 2-7: Vickers Hardness Test setup .....                 | 52 |
| Figure 2-8: Porcelain Bonded .....                            | 55 |
| Figure 2-9: Shear Bond Strength Test Setup .....              | 56 |
| Figure 2-10: Sagittal Plane Surface Deviation Analysis.....   | 58 |
| Figure 2-11: Transever Plane Surface Deviation Analysis ..... | 59 |
| Figure 2-12: Optical Microscope Image setup .....             | 61 |
| Figure 3-1:Bar graphs showing the mechanical properties.....  | 64 |
| Figure 3-2: Bar graphs representing Vickers Hardness .....    | 65 |
| Figure 3-3: Bar graphs representing Shear Bond Strength ..... | 66 |
| Figure 3-4: Bar graphs shows the mechanical properties .....  | 68 |
| Figure 3-5: Qualitative data .....                            | 69 |
| Figure 3-6: Optical images of the abutment .....              | 71 |
| Figure 3-7: Optical images of the connector.....              | 72 |
| Figure 3-8: Bar graphs showing the surface deviation .....    | 73 |



## List of Appendices

|  |     |
|--|-----|
| Appendix A-1: Windows view for the image of micro-CT and Control view display..... | 94  |
| Appendix A-2: Control view commands bar and view display.....                      | 94  |
| Appendix A-3: Control view setup screen.....                                       | 95  |
| Appendix A-4: Auto-conditioning the CT.....  | 95  |
| Appendix A-5: How to select the CT and running the machine.....                    | 96  |
| Appendix A-6: Select the data base name and run the position and optimize bar..... | 96  |
| Appendix A-7: Parameters setup for the CT-image.....                               | 97  |
| Appendix A-8: Correction shade setup.....  | 97  |
| Appendix A-9: Image view window display.....                                       | 98  |
| Appendix A-10: Acquired data set and CT-run.....                                   | 98  |
| Appendix B-1: The image tab processing.....  | 101 |
| Appendix B-2: Center of Rotation Setup.....  | 101 |
| Appendix B-3: Beam Hardening setup.....  | 102 |

|  |     |
|--|-----|
| Appendix C-1: Opening/Importing a Volume File .....  | 104 |
| Appendix C-2: Select the file volume.....  | 105 |
| Appendix C-3: Changing the file size and volume under the load file.....                                   | 105 |
| Appendix C-4: The histogram grey scale border.....   | 106 |
| <br>   |     |
| Appendix D-1: ROI and the Iso-surface properties.....  | 111 |
| Appendix D-2: (a) 3D color plot, (b) Comparison between the reference and test, (c) 2D<br>comparison ..... | 112 |

# Chapter 1

## 1 Literature Review and Background

### 1.1 Overview

Over the last thirty years, additive manufacturing (AM) or three dimensional (3D) printing has expanded for routine use in manufacturing processes [1]. AM fabricates an object by building material up rather than removing it [2]. It has the potential to be beneficial for the manufacturing industry due to low cost of the manufacturing, fast production, less waste material, and ability to fabricate components with complex structures [3].

There are a variety of materials used in AM such as polymers, composite, ceramics and metal alloys [2]. With this diverse group of material options, AM has impacted the aerospace, automotive, architecture, food and healthcare industries. With regards to the healthcare and dental industries, there is increasing interest in AM of metal alloys, due to the increased strength, as well as their established biocompatibility.

AM's success in the biomedical sector is evident based on its extensive application. It has been used for fabricating orthopedic prostheses and dental implants, both of which are replacements to tissues and interface with body parts [4]. As well, AM technology can be used for medical modelling to produce a 3D anatomical model (i.e., tissue or organ model) [5], by using the original medical image of the anatomy of interest, converting it to a surface model file, and printing the final 3D structure.

## 1.2 Additive Manufacturing (AM)

### 1.2.1 Definition of Additive Manufacturing

The American Society for Testing and Materials (ASTM) F2792-10) defines additive manufacturing as “the processes of joining materials to make objects from 3D model data, usually layer upon layer, as opposed to subtractive manufacturing technologies” [3]. It is also known as Rapid Manufacturing or Rapid Prototyping (RP) manufacturing, to describe the fabrication of any complex geometry components provided as a 3D model, developed without tooling components [6].

### 1.2.2 Additive Manufacturing in Dentistry

AM has the capability of producing and customizing parts that fit the patient’s anatomy. As such, it has direct application to the field of dentistry, which is evident by the recent demand for 3D printing technology for fabrication of dental devices [7]. There are different AM systems used in dentistry. Selective Laser Melting (SLM) is one such system and will be the focus of this thesis.

SLM is used for the production and fabrication of metal dental prostheses and restorations [13]. SLM is different from the computer-aided design and computer-aided manufacturing (CAD/CAM) subtractive method of milling. SLM creates 3D objects layer by layer through selectively melting metal powder with a laser beam [9]. It can be used to fabricate dental restorations and prostheses with complex geometries[16]. AM has been compared with the conventional techniques of dental restoration fabrication, which include casting and milling. SLM products showed higher metal porcelain bond strength and revealed better

results in corrosion and surface properties [9]. The SLM technology enhanced fabricating versatility, upgraded material properties, and a simplified production processes [15].

### 1.2.3 Benefits of Additive Manufacturing in Dentistry

AM has many benefits in its application within Dentistry. These include:

#### 1.2.3.1 Shape Complexity

Conventional manufacturing depends on cutting and slicing technologies to produce a limited number of shapes and structures [12]. For complex hollow structures, several parts need to be created and assembled. However, with AM technology, complex parts could be built from pre-designed structures [12]. Complexity of the structures could influence the shape and geometry in additive manufacturing [13]. Such complex structures are directly applicable to the dental field since personalization and customization of different designs, shapes, and sizes of dental prosthetics are required to fit the patient's anatomy.

#### 1.2.3.2 Functional Complexity

AM allows insertion of components like sensors and deposits of conductive materials. In biomedical applications, implants may take advantage of embedding functional components [2]. In addition, AM technology helps to customize medical devices and implant designs for the certain indications where patients are outside the standard range of the implant size and design, or for high-level surgical procedures where a single fitting is required for sufficient matching to the anatomical structures [14].

### **1.2.3.3 Time Efficiency and Less Manual Labor**

For complex structures, production using AM technology reduces the time for manufacturing. The result is the final product printed directly from CAD models, without the need for additional tooling or extensive post processing, thereby reducing the cost of production and ultimately having an impact on the supply chain by simplifying the manufacturing and assembly [2]. This is useful in dentistry, because the conventional casting procedure is a complex technique that involves several steps and materials, starting from making the wax pattern, investing, wax elimination, casting the metal, finishing and final polishing. Added to that is the dental technologist's time for each of the individual steps in the fabrication of a single crown or bridge [15].

### **1.2.3.4 Less Waste and Impact on Environment**

AM technology can have a positive impact due to less waste produced during manufacturing. Less material is used or needs to be recovered, since AM uses raw materials to build parts layer by layer. The leftover materials can be reused for the next processing, which has a lower impact on the environmental waste and reduces the cost in material [1]. This benefit is directly related to the comparison between AM and milling technologies used in dentistry. In AM, the part is fabricated layer by layer only using the material required. In comparison, milling is a subtractive manufacturing method that uses a cutting blade or sharp knife to remove material in the fabrication of the final part, producing waste materials and dulling the cutting blade side [16].

### 1.2.3.5 Design Iteration

Due to access to AM machines, device manufacturers can design components and print in hours. The printed object can then be used to get feedback on the device's performance [3]. If not satisfactory, the device design can be refined and reprinted with minimal cost and time for production. This could lead to better clinical designs and outcomes in dentistry.

### 1.2.4 Additive Manufacturing/3D Printing Processes

The AM process starts with modelling and runs through three main steps to create the final 3D object [17], as illustrated in the workflow below (Figure 1.1):

1. Data Acquisition: the models can be created through scanning or designing with Computer Aided Design (CAD) software.
2. Data Processing: the CAD file is converted to a stereolithography (STL) file. The STL structure is sliced by CAD software to create a bundle of layers.
3. Manufacturing/Printing: the object can be built layer by layer until the final object is created. Layer thickness is dependent on the machine parameters used.

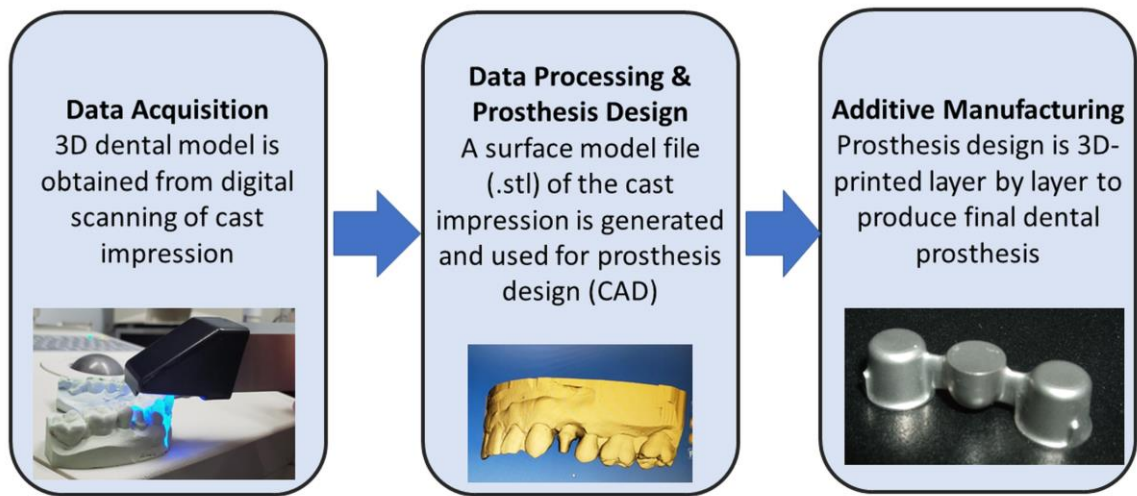


**Figure 1-1: Process flow for AM technique used in dental manufacturing**



## 1.3 Dental Prostheses Substructures

### 1.3.1 Types of Dental Prostheses

Fixed Partial Denture (FPD) is defined as “a dental restoration used to replace or restore the missing teeth, and that is permanently attached to adjacent teeth or dental implants”[18].

FPDs could replace a single missing tooth or multiple missing teeth.

#### 1.3.1.1 Crown

A crown is defined as “a cap to place on the head of the tooth, dental implant, or tooth substitute” [18]. As illustrated in the Figure 1.2.

The crown could be [19]:

- a. **Partial Crown:** a facing portion of the tooth structure to restore the width of one or more surfaces of the intact tooth. Materials used are ceramic or composite.
- b. **Full Crown:** a full and complete cover of the tooth structure that is used to restore multiple defective tooth surfaces and simulate the clinical crown of the tooth. There are three types which include the full metal crown, porcelain fused to metal and non-metal crown (only ceramic) cover.

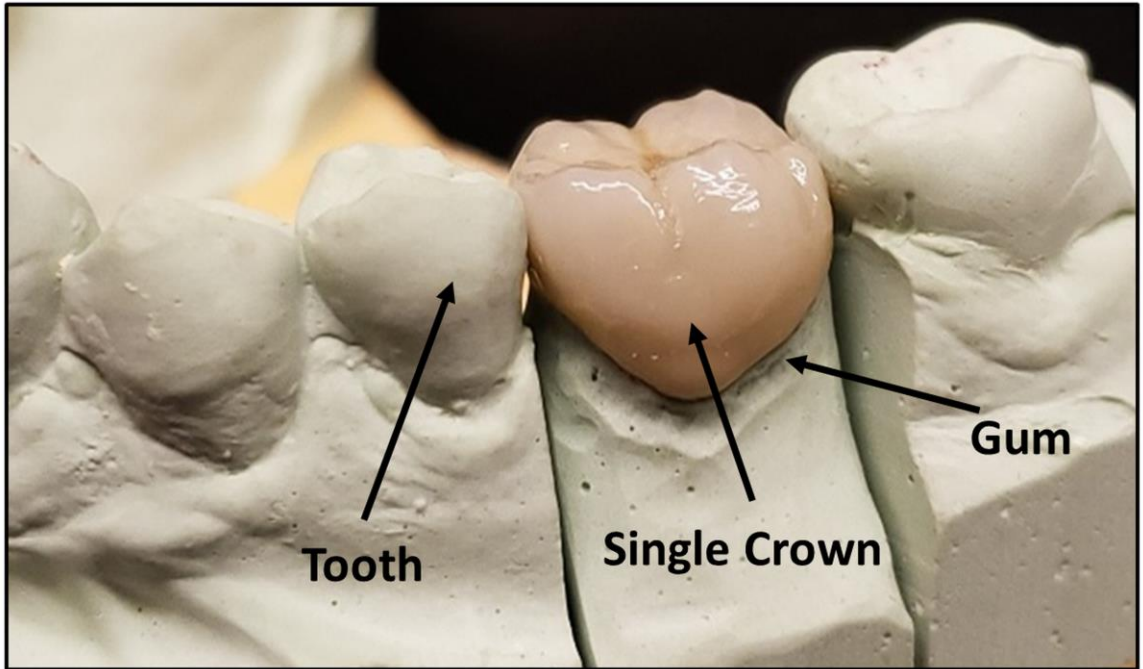


**Figure 1-2: Dental stone cast with single crown**

### 1.3.1.2 Bridge

As defined in the Glossary of the Prosthodontics Terms [18] “a bridge is a dental prosthesis that is luted, screwed, mechanically attached, or otherwise securely retained to natural teeth, tooth roots, and/or dental implants/abutments that furnish the primary support for the dental prosthesis and restores teeth in a partially edentulous arch; it cannot be removed by the patient”. A representative bridge is illustrated in the Figure 1.3.

The main components of the bridge design are described in Figure 1.4 [19]:

1. Abutments: adjacent teeth that will be prepared to support and lock the other components of bridge.
2. Pontic: the artificial tooth on the bridge that replaces the missing natural tooth and helps to restore the function.
3. Retainer: the main appliance that connects and unites the abutment teeth with the portion of the bridge.
4. Connectors: the secondary appliance that connect the retainers and pontics.

All these components play a major role in the bridge design and biomechanics. The superiority of the abutment and surrounding healthy bone play an important role in the successful design of the bridge [19]. If there are enough sound healthy abutments that support the missing teeth/tooth, the abutment should not transfer stresses to the pontic [20].



Figure 1-3: Dental stone cast with three-unit bridge

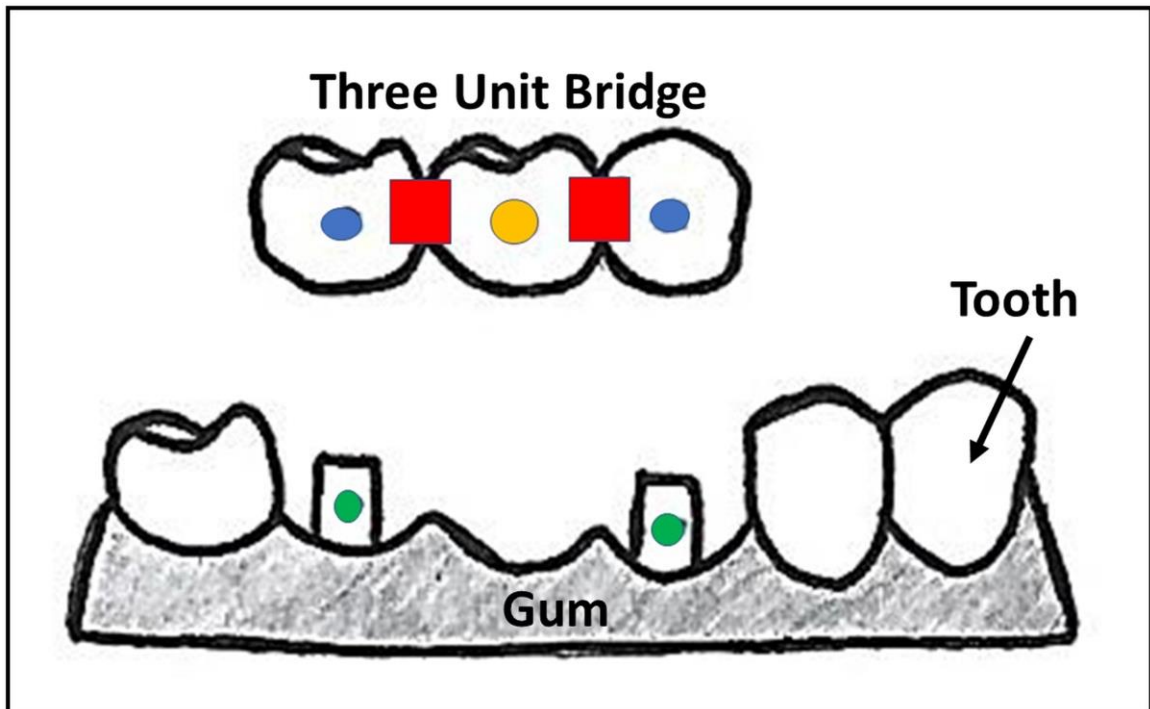


**Figure 1-4: Components of a three-unit bridge**

Colors in the image differentiate the components of the three-unit bridge: connectors (**red**), retainers (**blue**), abutments (**green**), and pontic (**yellow**).

### 1.3.2 Porcelain-Fused-to-Metal (PFM) Restorations

PFM restorations have been widely used as a type of porcelain dental restoration [21], as shown in Figure 1.5. They consist of many layers of different types of porcelain fused chemically to the metal substructures and provide support for the porcelain [22]. PFM restorations are the most popular dental restorations used, due to excellent mechanical properties, durability of the restoration to withstand wear and stress, in addition to their cost compared with other metal free restorations [22]. Additionally, PFM restorations have enough strength that can be used for the long span of bridges or for the posterior teeth restorations [28].

For a successful PFM crown, the preparation of the crown should meet the requirements of tooth reduction wherever the metal substructure is porcelain coated. One of the major challenges associated with the success of PFM's is selecting of an alloy and ceramic material with compatible physical properties that contribute to its bond strength and the natural appearance of the restoration.

#### 1.3.2.1 Porcelain-Metal Bonding

Dental porcelain should be able to chemically bond to the metal substructure. In case bonding does not occur, the porcelain layer will fail due to its brittleness [24]. When that occurs, the clinician assesses potential fractures, or any de-bonding of the porcelain layer from the PFM restoration. This failure will reduce the aesthetic of the restoration and create stains in the affected area and therefore repair of the restoration maybe required [25].

Bonding of porcelain to metal occurs as a result of an oxide layer being formed on the metal surface [23]. Therefore, the alloys for the PFM restoration need a special formula to help formation of the oxide layer. When the porcelain layer is fused onto the oxidized alloy surface, the chemical reaction between the oxide layer of the metal and the porcelain creates an interfacial bond between the porcelain and the metal [23].

Failures of the porcelain metal bond can occur as a result of several reasons [24]. For example, the metal may have an inadequate oxide layer, which leads to the delamination of the porcelain due to insufficient bonding. On the other hand, if the oxide layer is thick, it will be highly porous and full of defects, and failure will occur at the oxide interface [25]. When the oxide layer thickness is a molecular scale, failure will take place within the ceramic itself, near to the metal-porcelain interface. Researchers believe that microscopic cracks develop and grow gradually in the area of high stress or where bonding is non-existent between the porcelain and the metal [23]. When the cracks propagate, catastrophic failure occurs at the interface, and the porcelain will be delaminated from the metal.

A good bond between the porcelain and metal is achieved when there is proper matching between the coefficients of thermal expansion of the porcelain and metal [24]. The most ideal way to make a desirable matching bond is by selecting a porcelain with a coefficient of thermal expansion slightly less than that of the metal [25]. This allows for the metal to expand more during heating, and contract during the cooling process. The critical requirement for proper matching of the coefficients of thermal expansion of porcelain and metal means that not every type of porcelain is compatible [23] with dental casting alloys. Therefore, following the manufacturing materials and handling guidelines, to determine

casting alloys that are compatible with porcelain type, is important for preventing any failures of the bonding [23].



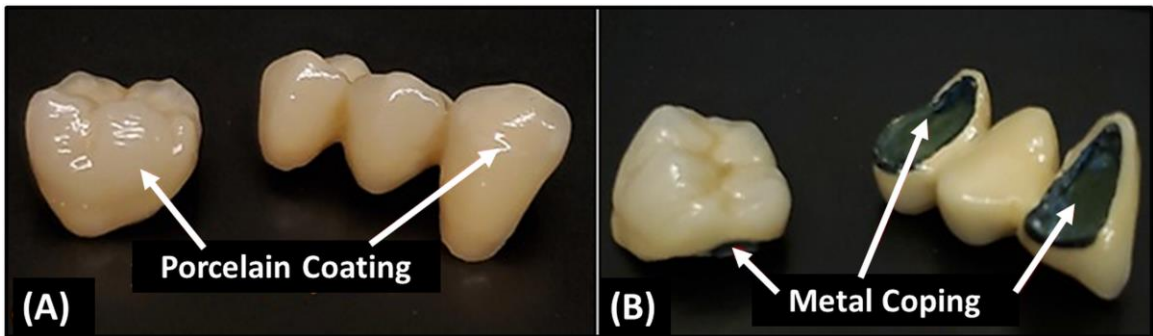


**Figure 1-5: Porcelain-fused-to-metal (PFM) restorations**

(A) Porcelain layer for a single crown (left) and three-unit bridge (right). (B) Metal coping shown for a single crown (left) and three-unit bridge (right).

### 1.3.3 Fabrication of Dental Prosthesis Substructures

#### 1.3.3.1 Lost Wax Technique

Casting of the metals are made by fabricating or constructing a hollow mold, pouring the molten metal that allows the metal to solidify, and separating the new solid cast metal from the mold [26]. All the metallic contents originate from casting. The cast metals used in the dental field replace or restore teeth and construct the removable or fixed denture framework. The framework supports and stabilizes porcelain crowns and bridges such that the fixed partial denture is strong while accommodating esthetic materials [27]. The casting processes is used to fabricate many types of dental restorations such as inlays, onlays, full cast crowns, porcelain fused to metal crowns, ceramic crowns and partial dentures [23]. The porcelain fused to metal is the most commonly used restoration on the market.

After the casting process is completed, the next step is to apply the porcelain layer on top of the metal surface. The porcelain is composed of primary contents such as silica ( $\text{SiO}_2$ ), feldspar ( $\text{K}_2\text{O} \cdot \text{Al}_2\text{O}_3 \cdot 6\text{SiO}_2$ ), and alumina ( $\text{Al}_2\text{O}_3$ ) [23]. These crystallization ingredients are heated together with fluxes such as sodium carbonate or lithium carbonate [26].

Main steps for the casting techniques [25-26], are shown below (Figure 1.6).

1. Producing the wax pattern: The wax pattern is an object to be cast produced. When the wax pattern forms on a die of the tooth or cast of the arch it accurately replicates the tooth structure.

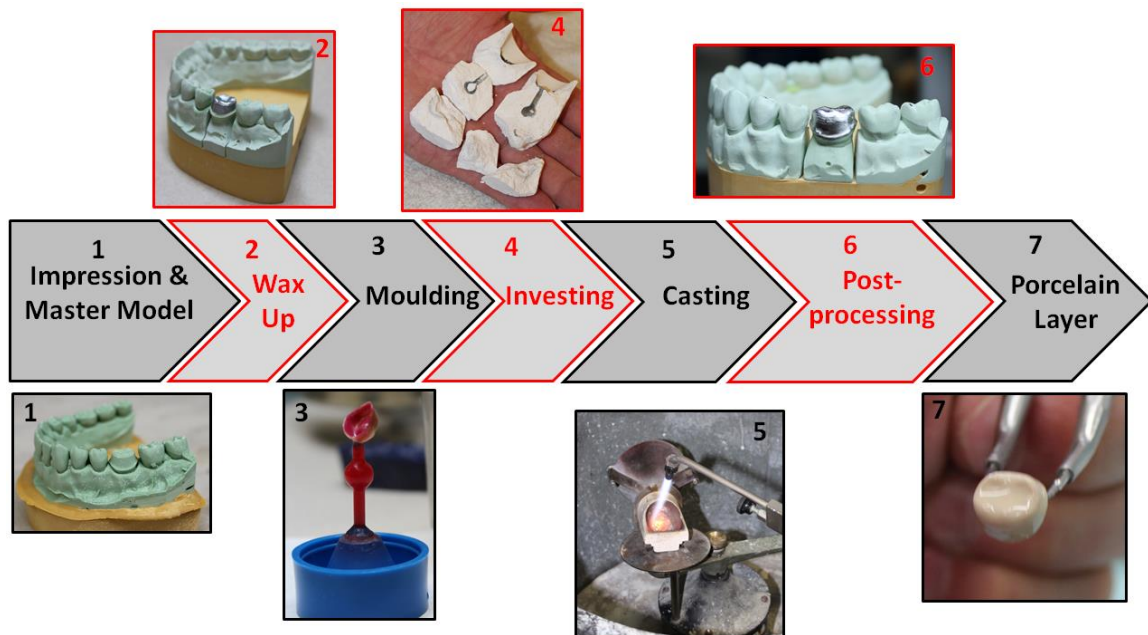


**Figure 1-6: Lost wax technique for dental casting**

The figure shows the various steps of the lost wax technique, from the initial patient impression to the final porcelain layer applied to the dental coping. (Image provided with permission by Mr. Milko Lamos RDT, University of Western Ontario, London, Canada)

2. **Spruing the pattern:** Spruing is a material that forms a channel for molten metal that allows it to travel through the channel and make the restoration. In the simplest case, the sprue is usually placed on the top of one cusp. If the case is complicated, then multiple sprues are placed. The other end of the sprue is attached to the cone of the sprue base. This cone helps to form a depression that allows the investment materials to guide the molten metal through the sprue hole.
3. **Investing:** Investing surround the wax pattern and sprue with a stone like product; this material can withstand the high temperature and forces during the burnout and casting. Investments are made from a binder that holds the investment materials together, and a refractory material which resists the heat produced from the burnout and casting. The investments from the wax pattern are very critical to the success of the casting. To retain the investment, a casting ring is used to place the sprue base. The investment material is mixed with power driven vacuum mixer. The water is added to the powder mixture in the bowl and sprinkled to eliminate air trapped. The lid is applied to the bowl and vacuum is attached to remove the air. The materials are poured slowly into the casting ring and loaded around the wax pattern without forming any bubbles or voids.
4. **Burnout the wax:** When the investments are completed, the ring is placed into the oven to burn out the wax pattern and the sprue. The burnout produces the hole that will be lifted in the investments where the wax pattern and sprue were before, making the space for the molten metal to flow and pass through it.
5. **Casting the materials:** casting is the process of the heating and changing the shape of the wax pattern then converting into cast metal. To accomplish the casting

process a centrifugal force machine is used. This machine allows the metal to be accelerated outward by spinning it rapidly. The metal is heated in a crucible made from ceramic that can resist the heating process. The substances called “flux” is added to ensure the metal melts without excessive formation of an oxide, which will affect the final product and quality of the casting. When the metal is melted completely, the hot casting ring is placed inside the crucible containing the melting metal and the crucible ring assembly is spun rapidly. The metal inside the crucible is accelerated into the space that was occupied before by the sprue and wax pattern. The metal piece to be cast is then heated by a blowtorch or electric current. The most common heating method for low temperature metal (<1200°C) is the blowtorch.

6. Removing the investment and cleaning: The casting is broken out from the investment and rinsed off with water. Cleaning of the investment materials is required to prepare the cast for the next steps.
7. Pickling: The surface of the cast restoration will be covered with a surface oxide layer, observed as dark appearance. This oxide layer can be easily removed by placing in an acid solution, which is called pickling. The casting is handled with insulated tongs and submerged in a boiling hot sulfuric acid for 5 to 10 seconds.
8. Finishing and polishing: After all the previous steps, the casting is ready for finishing and polishing processes. First is removing the sprue from the restoration attachment by using thin carborundum disk on a handpiece. Any rough and gross surface should be re-contoured by using the coarse carborundum stone or greenstone. After the re-contouring, the surface of the restoration should as smooth

as possible. Then a series of polishing steps are applied, starting with the rubber wheels and impregnated abrasive. After polishing is completed, the restoration should be a high luster appearances and smooth surfaces.

9. Applying the porcelain layer: In general, the metal is thinned to less than 0.5 mm to maximize the room for the porcelain. The crown is then degassed in a porcelain oven. The degassing is the process to remove the impurities at the alloy's surface and to form an oxide layer on the metal surface. After degassing, layering techniques are used to apply the porcelain, which hides the color of the metal substructure.

Limitation of the lost wax casting procedures can be classified in four categories [25, 27]:

1. Distortion: Any sign of distortion marked is related to the wax pattern distortion. It is the most common problem when forming and removing the pattern from the tooth or die. This mainly results from occluded air in the pattern, physical deformation (molding, carving or removal), release of stresses (trapped) during cooling, excessive storage time and high temperature during storage.
2. Roughness of the surface and irregularities: This is the most critical point for the casting processes because the surface of the dental casting should be accurate and replicate proper the surface of the wax pattern from which it is made. When the outer surface has excessive roughness, it can be solved by using additional finishing and polishing.
3. Porosity: This happens within the interior region of the casting or on external surface. The internal porosity weakens the casting and on the surface causes discoloration.

4. Missing or incomplete details: The cause of the incomplete casting is due to the molten alloy being prevented from filling the mold.

### 1.3.4 CAD/CAM Milling Technology

The milling system consists of three major components [34-35], which comprise the processes for the CAD/CAM technology Figure 1.7:

1. Scanner: Scans the dental preparation provided by the dentist and can be intraoral or extra-oral. For a single crown, the surface data for the tooth being prepared is scanned. For FPD frameworks, additional occlusal characterization is required, such as data acquired from the adjacent teeth and the opposing dentitions, as well as centric occlusion.
2. Software/CAD: Used for the 3D planning and design of the restoration. The software program helps with designing the virtual restoration on a virtual working cast, and then computing and digitizing the data for the milling parameters.
3. Hardware/CAM: Computerized milling device used for converting the virtual restoration into the final dental restoration from a solid block of metal or ceramic. It comprises primarily of the computer used for controlling milling. As a basic rule, after the CAM fabrication, some manual correction should be applied, and final polishing with staining colors or veneering materials are required to be carried out on by the dentist or dental technician.

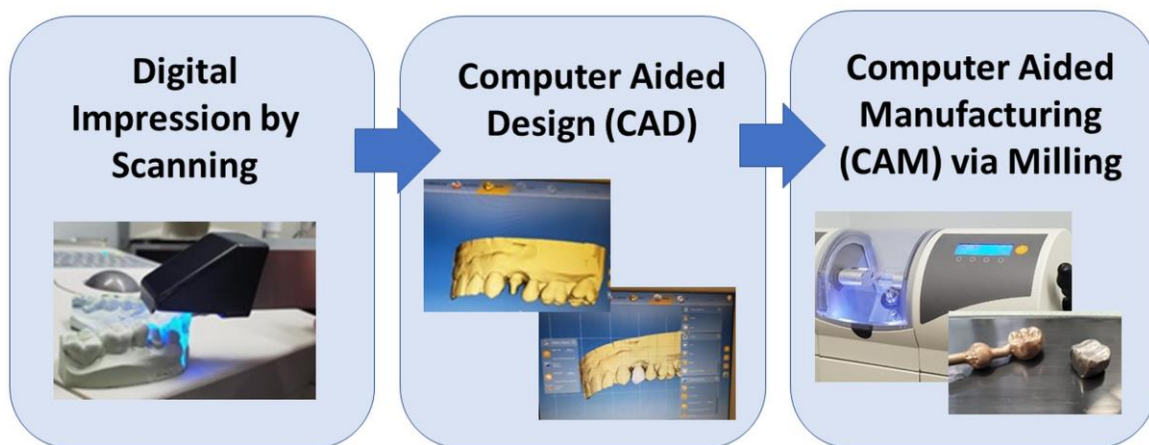


**Figure 1-7: CAD/CAM milling technique**



There are many advantages of using the CAD/CAM milling system for the fabrication of crowns and FPD's:

1. Reduced manual labor [28]: Compared to conventional casting, CAD/CAM milling has a reduced number steps for fabrication of dental restorations, especially those requiring a dental technician
2. Quality control [29]: Milling by CAD/CAM allows for quality control of dental devices. Firstly, it allows optimal device designs based on the material characterization defined by the CAD software. This prevents degradation by accounting for residual strain because of the post-processing. Secondly, it provides reproducible processing times for devices. Added to that, milling prefabricated ceramic or metal blocks used for milling contain minimal internal defects or porosity, as confirmed by the manufacturer.
3. Reduced time/cost at appointments [30]: Milled restorations only need one clinical appointment for completion. This eliminates the need for temporary or provisional restorations (*i.e.*, re-cementation or lost temporaries), and additional laboratory fees.

While there are advantages associated with CAD/CAM milling, there are also disadvantages:

1. The initial cost of the equipment and software is high, and dentist needs to spend more time and money to learn how to use this equipment. Added to that, without a large enough volume of restorations, dentists will face a hard time making their investments pay off [31].

2. Optical scanning is required to achieve an accurate representation of the tooth of interest. The scan needs to emphasize a good finish line and duplicate the surrounding occlusal teeth. In addition, some digital scanners need soft tissue management, retraction, and moisture control [32].
3. The digital impression system may not save time since it requires multiple steps; the dentist must first send the images for the clean-up, followed by setting of the margin by dental technologist. Then, the image is sent to the dental laboratory for checking the quality of the impression. The completed models and dies are then sent to the dental lab for final fabrication processes [33].

### 1.3.5 Metal Additive Manufacturing

Dentistry is one avenue in medical manufacturing that can benefit from AM. Artificial teeth, dental implants, and prosthetics devices can be fabricated rapidly, sometimes within the dental office [14]. The prosthodontics field can benefit from AM technology, specifically for the fabrication of fixed partial denture (FPD) and removable partial denture (RPD) systems. RPD's are simple and cost effective prostheses that can restore the missing teeth in the partially edentulous patients [34]. RPD frameworks are commonly made of Co-Cr alloys because of their suitable mechanical properties, excellent corrosion resistance and biocompatibility [34]. Traditionally, RPD's frameworks were fabricated by the lost wax technique (casting techniques), but then progressed to fabrication with the CAD/CAM milling system. Currently, metal AM is being explored for fabrication of RPD frameworks [35].

Cobalt-chromium (Co-Cr) and titanium (Ti-6Al-4V) are the most commonly used metal alloys for metal AM in dentistry [36]. They are available as a powder form, with particle sizes ranging between (20 – 100  $\mu\text{m}$ ) [36], [37]. Depending on the manufacturer, composition of the powder may vary [38], [39]. Metal AM is suitable for the fabrication of FPD substructures and RPD frameworks because Co-Cr alloys are considered the best dental base metal in terms of the cost, biocompatibility, handling, mechanical properties, and the clinical performance [40].

#### 1.3.5.1 Selective Laser Melting Technology (SLM)

SLM is a specific type of AM technology designed to use a high energy laser to melt and fuse metallic powders [10]. SLM is classified as a powder bed fusion process, utilizing a high energy laser to melt metal powders layer by layer to produce the final 3D part based on the CAD file geometry. Before uploading the CAD data to the SLM machine for printing, the CAD file requires conversion to an STL file to produce slice data for laser scanning of each layer [41]. The SLM machine used in this study was manufactured by Renishaw (AM 400, Renishaw, Staffordshire, United Kingdom).

The SLM process is initiated by laying a thin layer of powder on the substrate plate [62]. A high energy laser is used to melt and fuse the metal powders according to the CAD data fed to the machine in the X-Y axes, followed by a second layer of powder placed on the plate [41]. The process is repeated until the part is fabricated into the desired geometric 3D shape. The build chamber is completely sealed as it's necessary to maintain a precise temperature for melting of the powder materials [49]. At the end of the build, the excess

powder is cleaned, removed and recycled and the part is detached from the substrate either manually or electrically [41]. Figure 1.8 shows the schematic for the SLM process.

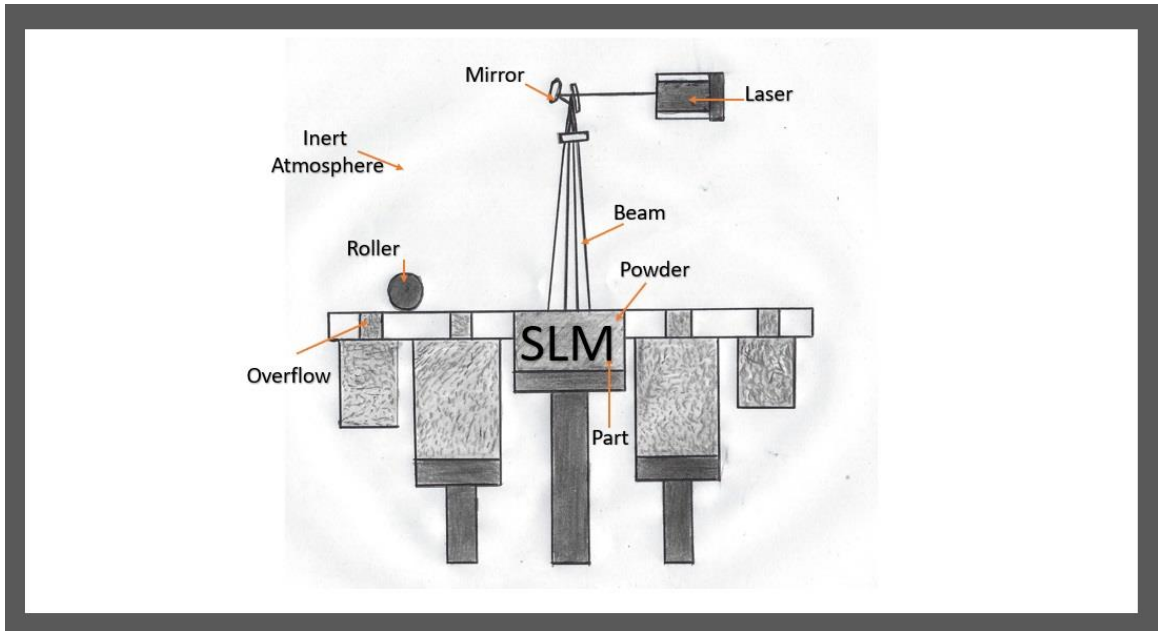


**Figure 1-8: Schematic of the selective laser melting (SLM) process**

The SLM process occurs in an inert, heated atmosphere. The alloy powder is coated onto the build platform using a roller, based on a specified layer thickness. A high-powered laser melts the alloy powder specific to the part layer geometry. This entire process is repeated layer by layer to fabricate the final 3D-printed part.

(Notes: Dr. Kalman, he thinks this figure is confused)

Some advantages of using SLM technology [42]:

1. The use of a range of different materials
2. The capability to tune properties during the fabricating of parts
3. Improved functionality
4. Moderately low cost
5. Manufacturing of net-shaped components that will be ready to use

On the other hand, SLM has some drawbacks such as [42]:

1. The processing technique is quite slow (because of the process speed limitations)
2. Critical size limitations
3. High power usage
4. Initial high costs
5. Time consuming for parameters process optimization
6. The handling of the powder can be delicate which are very fine particles
7. The final products surface can be rough (related to the powder particle size and the system parameters) [42]
8. Fragile and high temperature materials that cannot tolerate the high internal stress throughout the manufacturing process can crack. This can be overcome by reducing the cooling rate (by engaging substrate plate heating) [43]. At the same time, this could lead to anisotropic microstructure in the material along the building processing direction [42].

### 1.3.5.2 Dental Alloys Used in Metal Additive Manufacturing

Metal alloys have been used as the material of choice for prosthodontic restorations for the last 25 years [44-45]. The metallic materials are applied for the internal and external structures and components of many prosthetic restorations [46]. Nowadays, there are a number of metals used in prosthetic fabrication which include gold, palladium, silver, nickel, cobalt, and titanium [44].

Alloys are metallic material formed from two or more metals, or from metals with non-metals [25]. Metal alloys have favorable properties that make them suitable for handling and manipulation. These include their high elastic modulus and good loading capacity that make them desirable for dental applications [46]. Added to that, they are biocompatible, resistant to corrosion, have high static and dynamic strength, high toughness, and show no evidence of metal ion release into the oral cavity environment [46].

#### 1.3.5.2.1 Non-Precious Dental Alloys

This group of alloys is based on the non-precious metals, such as chromium, nickel, iron, tin, lead, magnesium and titanium [24]. These alloys were introduced as an alternative to gold alloys because of the significant increase in gold prices. Generally, non-precious alloys are economical and have good physical, chemical and mechanical properties. Non-precious dental alloys that are commonly used include nickel chrome (Ni-Cr), cobalt chrome (Co-Cr) and titanium (Ti) based alloys [24].

#### 1.3.5.2.2 Titanium (Ti) and Titanium-based Alloys

Titanium and titanium-based alloys are commonly used in dentistry [25] due to their excellent biocompatibility, lower density and mechanical properties compared to the other non-precious dental alloys [24]. They can be used for all-metal and metal-ceramic prostheses, as well as dental implants.

Ti has a high melting point (1668°C) and high rate of oxidation above 900°C. For the metal-ceramic prostheses, the porcelain is sintered at temperatures below (800°C), which is good to minimize the oxidation, and prevent the alpha phase from converting to the higher beta  $\beta$  phase [24]. The high melting temperature of the Ti alloys makes them highly resistant to sag deformation within the metal frameworks at the porcelain sintering temperatures.

#### 1.3.5.2.3 Cobalt Chrome (Co-Cr) Alloys

The invention of proper casting techniques and materials for making models resistant to high melting temperatures was made possible through the use of Co-Cr alloys in dentistry [12]. The application of Co-Cr alloys in dentistry is constantly growing due to their superior mechanical properties, lower density and cheaper than gold alloys [47]. These alloys exhibit high melting temperatures and therefore require special casting devices which make their application rather difficult. Co-Cr based alloys are commonly used for making dental prostheses such as removable partial dentures, crowns and bridges in metal-ceramic systems [12]. They also exhibit good bond strength with porcelain, higher mechanical properties, lower density and superior corrosion resistance compared to other metal alloys used in prosthodontics [12].



Cobalt possesses good corrosion resistance and can be used in multi-phase alloys to improve their mechanical properties [46]. Chromium is the primary alloying element in a wide variety of cobalt super alloys and is preferably added to improve corrosion resistance.

The main composition of cobalt chrome alloys for metal-ceramic restorations by their weight percentage (wt.%) and characterizations for each element are as follows [46]:

1. Cobalt (Co): when added to the palladium alloys, it results in an increase in the thermal coefficient of expansion and an improvement in the mechanical properties. The percentage weight of Co in cobalt based alloys is around 55-58%.

2. Chromium (Cr): it is the metal that helps improve the solidification solutions during the hardening stages. Because it has passivity effects that contribute to the corrosion resistance in nickel and cobalt based alloys, it also provides a good resistance to tarnish. However, the sigma phase in Cr makes the alloy brittle which can result in the fracture of the cast. As such, the percentage Cr is limited between 5 to 25%.

3. Molybdenum (Mo): helps improve the resistance to corrosion by forming the passive layer and have a beneficial effect on thermal expansion coefficient. The percentage Mo in Co-Cr alloys ranges between 0 to 4 %.

4. Aluminum (Al): added to the Co-Cr alloys to help in etching the surface of the alloys to create micromechanical retention for the alloy's surface. The percentage Al in Co-Cr alloys ranges between 0 to 2%.

5. Iron (Fe): added to the Co-Cr alloys for the metal-ceramic system for improved hardness and strengthening the bond of the oxygen to oxide layer. It also helps with enhancing the

processing ability of the alloys in the cold state. The percentage Fe in Co-Cr alloys ranges between 0 to 1%.

6. Gallium (Ga): added to the non-silver ceramics to reduce the coefficient of thermal expansion that's producing from the absence silver contents. The percentage Ga in Co-Cr alloys ranges between 0 to 7%.

7. Niobium (Nb): the metal element that provides a good corrosion resistance for Co-Cr alloys. The percentage Nb in the Co-Cr alloys ranges between 0 to 3%.

8. Tungsten (W): another name wolfram, same as Nb properties are good for resistance to corrosion. The percentage W in Co-Cr alloys ranges between 0 to 5%.

9. Boron (B): it is a deoxidization agent. It increases hardness of the nickel-based alloys, reduces the surface tension of the molten alloys, improves the castability, and reduces the ductility when it is added to the alloys. The percentage B in Co-Cr alloys ranges between 0 to 1%.

10. Ruthenium (Ru): a precious metal belongs to the platinum group. It is a grain refiner to improve the mechanical properties and resistance to tarnishing. The percentage Ru in Co-Cr alloys ranges between 0 to 6%.

## 1.4 Micro-Computed Tomography ( $\mu$ -CT)

### 1.4.1 What is Micro-CT?

CT is a scanning process used to produce three dimensional (3D) data that represents an object, by taking series of X-ray radiographs around a rotation axis, and then reconstructing a 3D model using algorithms [48]. Micro-CT is a system using a micro-focal spot X-ray source and high-resolution detector, to allow for more projections in multiple viewing directions, to produce 3D reconstructed images of samples or objects [49]. Micro-CT cannot be used with patients. The image is characterized as spatial distribution maps of linear attenuation coefficients determined by the level of the energy of the X-ray source and the atomic composition of the material sample [49].

Micro-CT has been used for different research applications in dentistry. These include the study of the dental material properties, dental anatomy evaluation, and marginal fit analysis for dental restoration [50]–[53]. Currently, micro-CT is being utilized as a tool for analysis of the internal structure of additively manufactured parts in the field of medicine and dentistry [54].

“Micro” indicates the pixel sizes of the image cross-sections are in the micro-meter range. The X-ray projections are then collected by X-ray panel detectors and reconstructed in computer software to produce virtual 3D models of the scanned object. Collection of data is affected by the x-ray absorption and scattering of the material. Hence a material that does not absorb x-rays will appear as radiolucent (darker appearance due to radiation easily passing through). The internal structures of the object are obtained by the x-ray projections

that penetrate the object. Thin scan sections are produced and can be used for structural analysis depending on the x-ray settings utilized [63]. Micro-CT is used in metrology to measure the dimensional quality of AM components in the metal industry [55]. SLM technology provides the versatility and capability to produce and fabricate full dense parts from metal powder and build it up layer by layer [56]. Micro-CT has high power energy to penetrate the dense metal produced by SLM and provide an image of the internal structures of the component. One such micro-CT scanner capable of scanning metal parts is the Nikon Micro-CT Scanner XTH 225 ST model shown in Figure 1.9.

There are many advantages of micro-CT imaging for research applications:

1. The imaging procedure is non-destructive which can preserve the samples for the other biological and mechanical test procedures [57]
2. Aids in analyzing the 3D relationship between internal structures [57]
3. Has high contrast resolution, which is higher than Cone-Beam Computed Tomography (CBCT), thus allowing excellent discrimination of very small differences in attenuation coefficient ( $< 1\%$ ) [57]

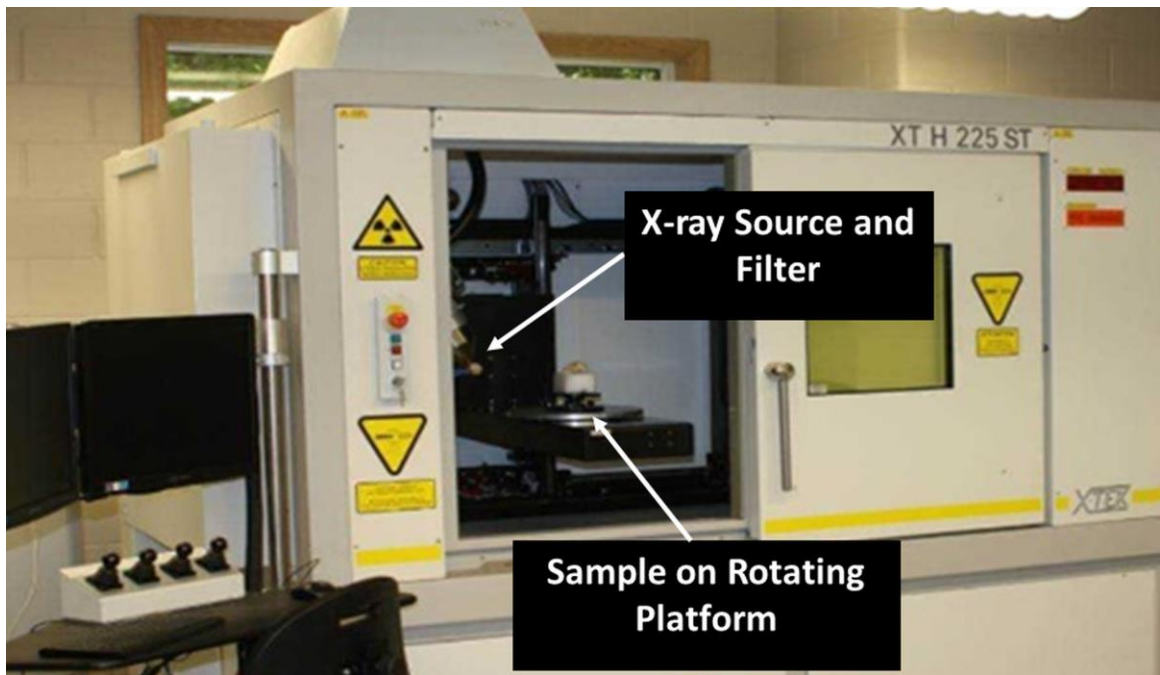


**Figure 1-9: Nikon micro-CT scanner (model XTH 225 ST)**

The Nikon micro-CT scanner is capable of imaging high density objects, such as the metal structures investigated in this thesis.

## 1.5 Study Rationale

Despite the advantages offered by additive manufacturing for dentistry, the Canadian dental industry is still on the verge of adopting metal AM in its routine fabrication of dental devices. This hesitance could be due to the lack of information in the literature regarding the performance of AM-fabricated dental devices. As such, it is necessary to explore metal AM relative to conventional forms of dental manufacturing in order to demonstrate its feasibility and success as a potential contributor to dental device fabrication in Canada. This thesis aims to evaluate metal AM as a manufacturing method for Co-Cr FPDs, by analyzing alloy samples and substructures fabricated using this technology and comparing the data to that obtained for similar samples fabricated using conventional manufacturing techniques. Therefore, the overall objective of the study is to directly compare dental substructures prepared using Selective Laser Melting AM technology to those fabricated with the conventional methods of waxing-casting and milling. The following were assessed; (i) material and mechanical properties; (ii) qualitative assessment of the internal porosity; (iii) porcelain adherence; and (iv) the geometric accuracy of fabrication.

## 1.6 Objective and Hypotheses

The specific objectives of the research were:

1. To evaluate mechanical properties of alloy samples fabricated using AM, milling and casting, and compare results of alloy strength, deformation, hardness, and bond strength with porcelain.
2. To compare three-unit dental bridge substructures fabricated using AM, milling and casting, for differences in flexural strength and deformation.
3. To investigate the internal porosity of three-unit dental bridge substructures fabricated by AM, milling and casting, using micro-CT imaging and metallurgic investigations for internal structure analyses.
4. To compare the geometric accuracy of three-unit dental bridge substructures fabricated by AM, milling and casting to the ideal surface design (CAD model).

Multiple hypotheses were associated with these objectives:

1. AM alloy samples will demonstrate equal or superior mechanical performance when compared to conventional cast and milled alloy samples.
2. AM alloy samples will exhibit equal or superior porcelain bonding when compared to conventional cast and milled alloy samples.

3. AM three-unit bridge metal substructures will show equivalent or superior fracture resistance (high flexural strength, low flexural deformation) when compared to conventional cast and milled metal substructures.

4. AM three-unit bridge metal substructures will demonstrate equal or improved accuracy of fabrication when compared to conventional cast and milled metal substructures.

## 1.7 Thesis Organization

The work presented in this thesis focuses on “*Metal Additive Manufacturing for Fixed Dental Prostheses*”.

### **Thesis Contents:**

*Chapter 1* presents the background and pertinent literature review of dental manufacturing techniques, material properties of alloys, and imaging methods used for assessing dental substructures.

*Chapter 2* presents the materials and methods for mechanical testing, assessments of fabrication accuracy, qualitative analysis for the porosity, and metallurgic analysis used to compare dental substructures fabricated by AM, milling or casting.

*Chapter 3* presents the results of mechanical testing, assessments of fabrication accuracy, qualitative assessment of the porosity, and metallurgic analysis of dental substructures fabricated by AM, milling and casting.



***Chapter 4 presents*** the discussion and conclusions obtained from the mechanical testing, assessments of fabrication accuracy, porosity, and metallurgic analysis, as they relate to the comparison of dental substructures fabricated by AM, milling or casting.

## Chapter 2

### 2 Materials and Methods

#### 2.1 Materials

##### 2.1.1 Cobalt Chromium (Co-Cr) Sample Design and Specifications

Forty-five rectangular Co-Cr alloy bar samples (50 mm x 15 mm x 2 mm) and twenty-seven Co-Cr alloy three-unit bridges were used for comparison of milling, casting and AM fabrication methods Figure 2.1. The rectangular bars were made according to specifications set out in American Society of Materials and Testing standards (ASTM-E290-97a) [58].

Three-unit bridges were made using a custom designed model, standardized for testing.

Rectangular bars and three-unit bridges made out of Co-Cr alloys were produced by Additive Manufacturing (AM) using Selective Laser Melting (SLM) technology (Renishaw AM400; ADEISS, Western University, London, Ontario, Canada), and the conventional methods of dental manufacturing; lost wax technique dental casting and milling technology (Rotsaert Dental Laboratories; Hamilton, Ontario, Canada).

Rectangular Co-Cr samples (n=45) were divided in three groups. Fifteen Co-Cr samples were assigned to each group; Cast Argeloy NP Supreme (Cast), Mill Kera®-Disc (Milled) and Additive Manufacturing (AM) (Co28Cr6Mo-LC, Gas Atomized Powder, UK).

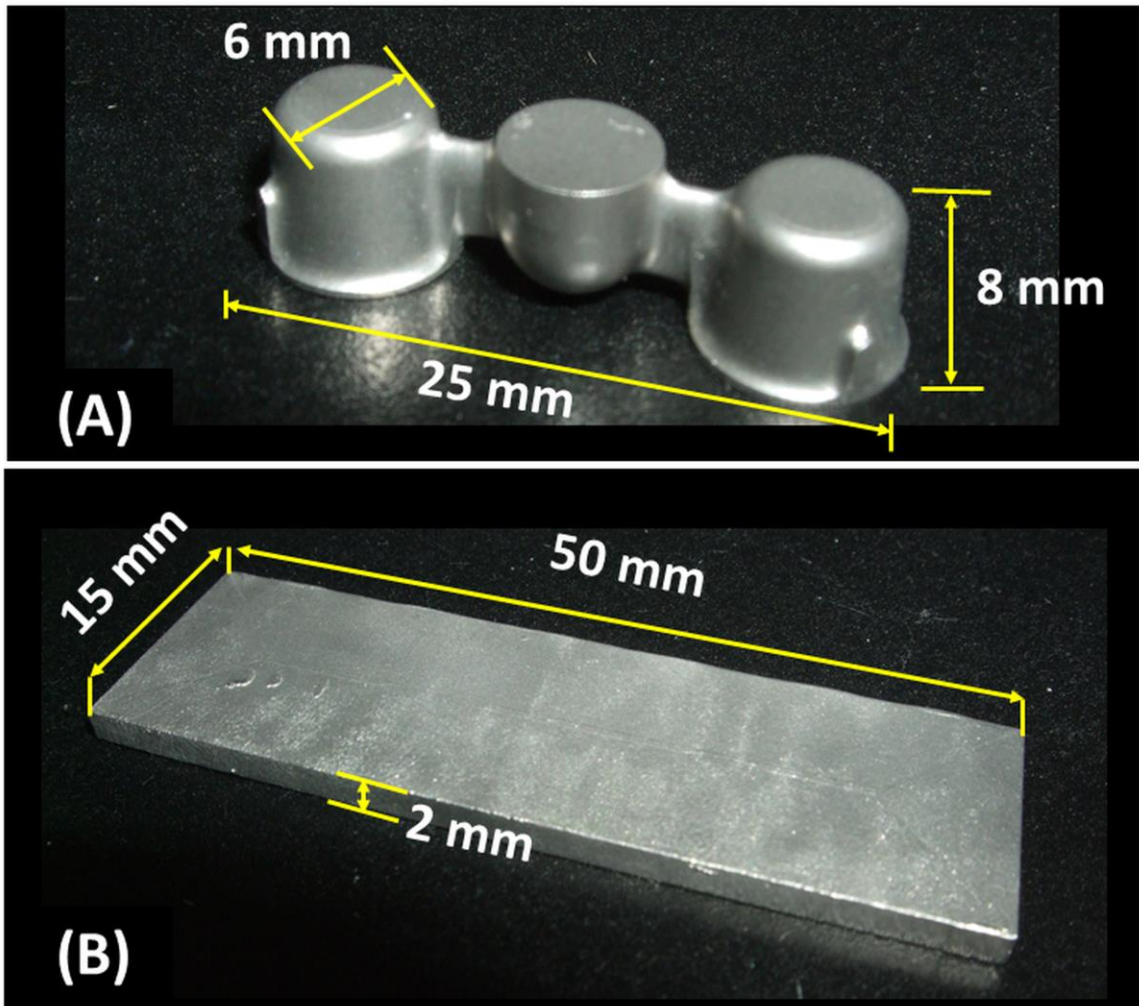


**Figure 2-1: Co-Cr sample designs used for mechanical testing**

(A) Three-unit bridge and (B) rectangular bar.

Three-unit-bridges (n=27) were divided into three groups, with nine samples assigned per group; Cast Argeloy NP Supreme (Cast), Mill Kera®-Disc (Milled) and Additive manufacturing (AM) (Co28Cr6Mo-LC, Gas Atomized Powder, UK). Materials specifications, handling, processing techniques and properties are described in Table 1 [56].

## 2.2 Methods

### 2.2.1 Fabrication of Rectangular Bars and Three-Unit Bridge Substructures

#### 2.2.1.1 Additive Manufacturing (AM)

For AM specimens, a 3D digital design (CAD model) was used to initiate the fabrication process. Once the design was processed by the SLM machine (Renishaw AM-400), a high powered and focused laser (70  $\mu\text{m}$  laser diameter, 200W laser power) was used to melt layers of Co-Cr alloy powder (Co28Cr6No-LC, Renishaw) with layer thickness of 40  $\mu\text{m}$  at a speed of 2 m/s. This resulted in consolidated metal specimens.

#### 2.2.1.2 Milling

For the milled specimens (Kera® Disc), the 3D geometries were digitized with CAD software, and the Co-Cr alloy block was milled. The final cut was made according to the dimensions of the digital design using a computerized numerically controlled milling machine (450i Imes-Icore) following the manufacturing manual [59] (Rotsaert Laboratory Hamilton, Ontario.)

Table 1: Chemical Composition of Co-Cr alloys for AM, Milling and Casting.

| WT<br>(%)*  | Co                             | Cr   | W    | Si   | Mo   | Mn   | Fe   | C    | Al    | B    | N    | Ni    | P     | S     | Ti   | O  | Other |
|---|--------------------------------|------|------|------|------|------|------|------|-------|------|------|-------|-------|-------|------|----|-------|
|   |                                |      |      |      |      |      |      |      |       |      |      |       |       |       |      |    |       |
| Balance   | 28                             | 0.02 | 0.57 | 6.10 | 0.77 | 0.20 | 0.02 | 0.06 | <0.01 | 0.22 | 0.05 | <0.01 | <0.01 | <0.10 | 0.03 | -  |       |
| Manufacturing (AM)<br>(Co28Cr6Mo-LC)  | 62                             | 27.8 | 8.22 | 1.54 | --   | 0.21 | 0.13 | 0.02 | --    | --   | --   | --    | --    | --    | --   | -- | <0.1  |
| Mill Kera®-Disc   | 61                             | 27   | 5    | 1    | 6    | --   | --   | --   | --    | --   | --   | --    | --    | --    | --   | -- | --    |
| Cast Argeloy NP<br>Supreme  | *Chemical composition/mass (%) |      |      |      |      |      |      |      |       |      |      |       |       |       |      |    |       |
| Co: Cobalt, Cr: Chromium, W: Tungsten, Si: Silicon, Mo: Molybdenum, Mn: Manganese, Fe: Iron, C: Carbon, Al: Aluminium, B: Boron, N: Nitrogen, Ni: Nickel, P: Phosphorus, S: Sulfur, Ti: Titanium & O: Oxygen. |                                |      |      |      |      |      |      |      |       |      |      |       |       |       |      |    |       |

### 2.2.1.3 Casting

Cast specimens were prepared using the wax elimination process at Rotsaert Laboratory (Hamilton, Ontario, Canada), using protocols for casting and investment according to the manufacturing materials and industry standards.

## 2.2.2 Imaging Analysis of Three-Unit Bridges

### 2.2.2.1 Micro-CT Scanning

Out of the forty-five three-unit-bridge specimens fabricated (n=15 per AM, Cast and milled groups), five specimens were randomly selected from each group and scanned to obtain high resolution  $\mu$ -CT images (Nikon, Micro-CT Scanner XTH 225 ST model; Museum of Ontario Archaeology, London, Ontario, Canada). A plastic holder was 3D printed to mount the three-unit bridge samples within the micro-CT scanner Figure 2.2. See Appendix (A) for further set up procedures. The plastic holder was designed to mount three samples per scan and minimize the setup and takedown in between scans. A custom fixture supported the plastic holder within the CT scanning machine.

The entire set-up (plastic holder and custom fixture) stabilized the samples while the stage moved during scanning. Images were obtained under specific micro-CT parameters; 220 kV beam energy to ensure full penetration through the Co-Cr samples, 50  $\mu$ A current, and 11-Watt power, with a voxel resolution 15  $\mu$ m. A copper filter (1 mm) was used during the scanning procedure to pre-filter the x-ray energy and help reduce the effect of beam hardening on the image quality.

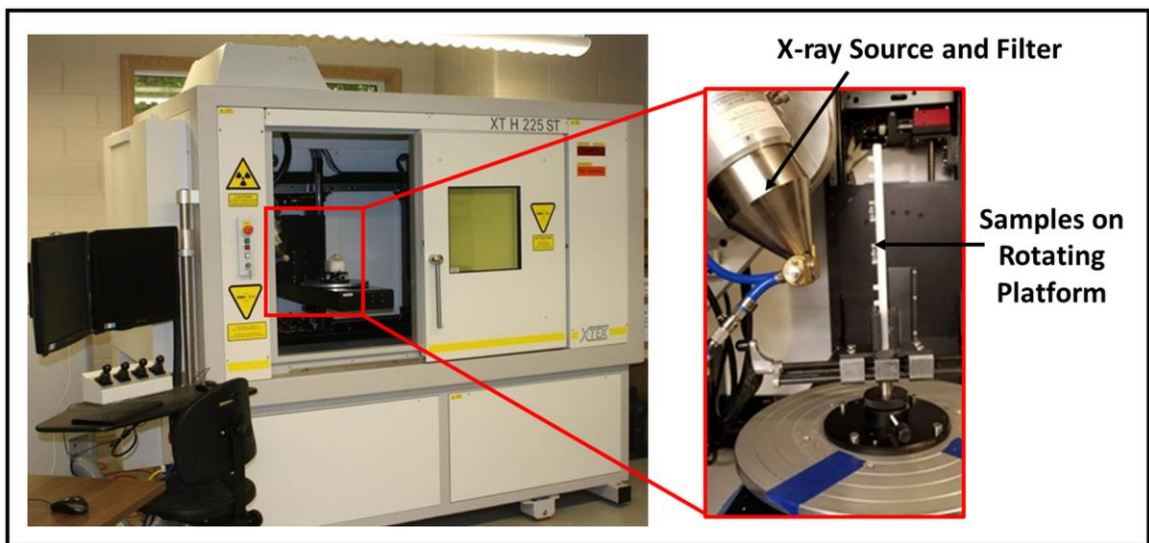


**Figure 2-2: Nikon micro-CT scanner (model XTH 225 ST)**

The Nikon system was used to obtain micro CT scans for CoCr three-unit bridge samples.

The half projection (1570) was performed for 26 minutes. When the scanning was complete, VG Studio Max 2.2 software (Volume Graphics Inc, Charlotte, NC, USA) was used for image processing and to generate a VGL file of the 3D reconstructed image (see Appendix B and C for details). Figure 2.3 describes the workflow of the micro-CT process.

## 2.2.3 Mechanical Testing

### 2.2.3.1 Bending Test

#### 2.2.3.1.1 Rectangular Bar Samples

The three-point bending test was conducted on forty five rectangular bar specimens (n=15 for each of Cast, milled and AM) according to ASTM standards (ASTM-E290-97a) [58] using a universal materials testing machine (Instron series 3345 University Ave, Norwood, MA, USA), with a 5 kN load cell at a crosshead speed of 1 mm/min. All bar samples were tested until fracture was reached. The direction of the load was perpendicular to the bar samples. The three-point bend test setup for the rectangular Co-Cr specimens is shown below in Figure 2.4. The flexural modulus for all samples was calculated using the following equation below [58]:

$$E_f = \frac{L^3 m}{4 b d^3} \quad (1)$$

Where,

$E_f$  = Flexural Modulus of elasticity (MPa)

$L$  = Support span length (mm)

$m$  = Slope of the force vs displacement curve in the elastic region (N/mm)

$b$  = Width of the test bar beam (mm)

$d$  = Depth or thickness of tested bar beam (mm)



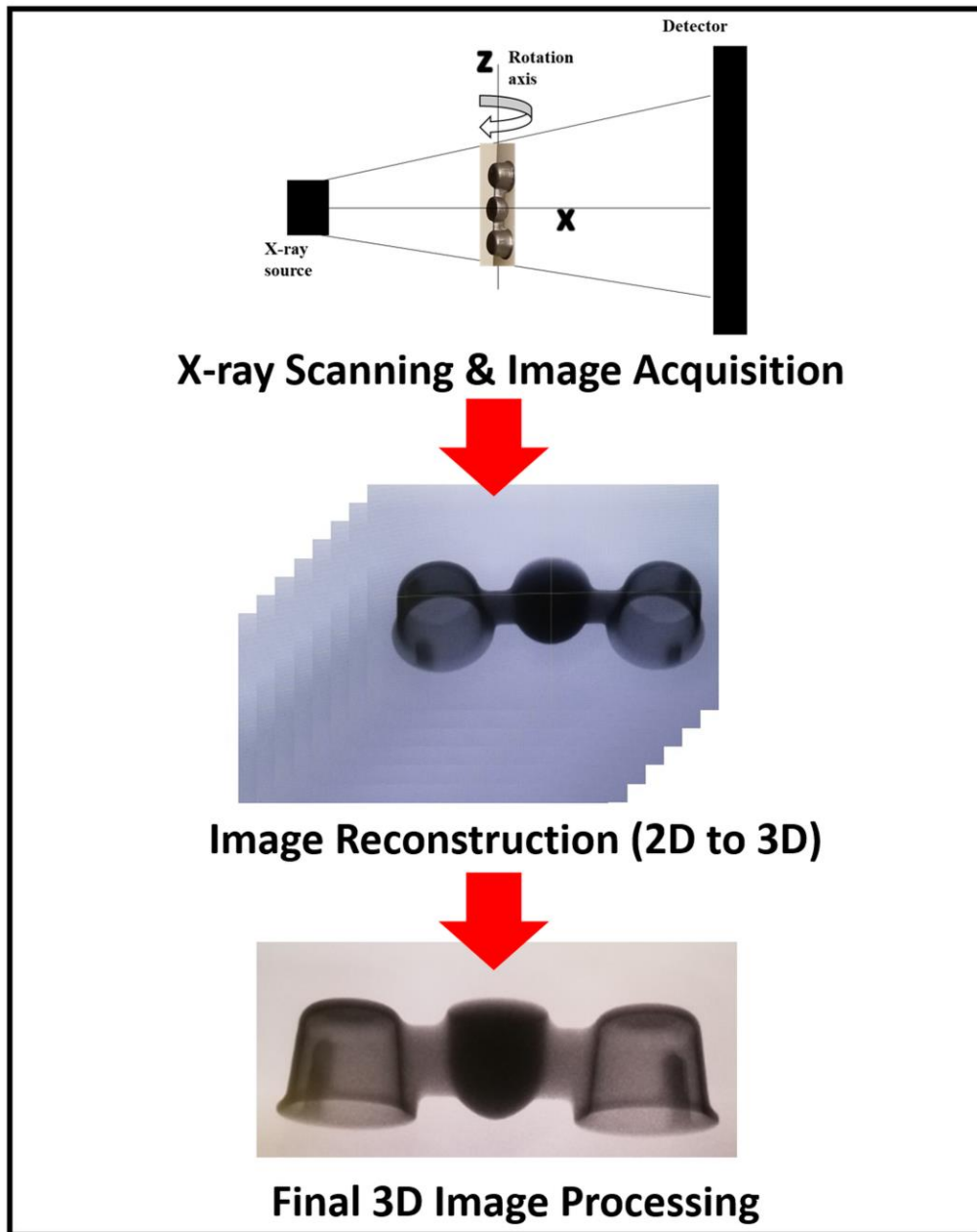
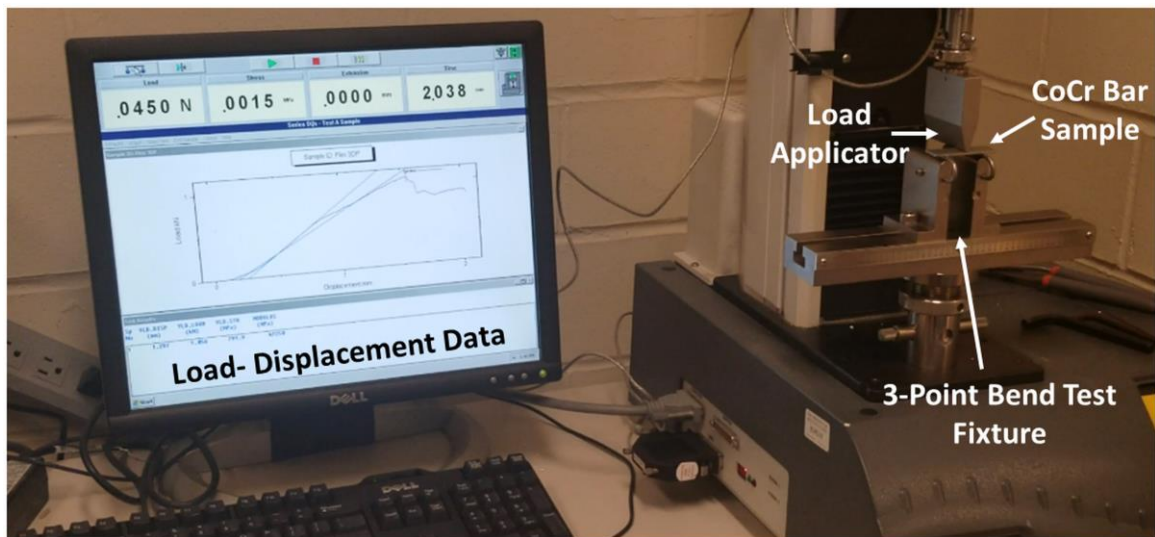


Figure 2-3: Workflow chart for the full micro-CT process



**Figure 2-4: Three-point bend test setup for the rectangular Co-Cr samples**

### 2.2.3.1.2 Three-Unit Bridge Samples

Similar to the rectangular bar samples, three-point bend testing of the three-unit bridge samples (n=9 for cast, milled and AM group) was conducted using a universal testing machine (Instron 8874 series Axial-Torsion Systems, INSTRON®, 825 University Ave, Norwood, MA, USA). A 10kN load cell was used, and the load was applied with a crosshead speed of 1mm/min until fracture occurred. The force at fracture was recorded. The three-unit bridge specimens provided in-vitro data to support the potential clinical performance of the alloy's substructures. The schematic setup for the three-point bend test for the three-unit bridges is shown in Figure 2.5.

### 2.2.3.2 Hardness Test

Post- bend testing, the rectangular bar specimens were sectioned in half, and fractured regions were eliminated, such that square samples (15 mm x 15mm) could be harvested Figure 2.6. Three square samples per group (AM, milled & cast) were used for hardness testing, and ten indentations were obtained at random areas of each sample. Prior to testing, each sample was ground under water using Buehler® Metaserv Grinding-Polisher (SR-98553) and silicon carbide papers at different grit sizes (400, 1000 and 2000).

Vickers hardness testing was conducted on the cast, milled and AM samples using an Omnie Met hardness testing machine (Buehler Lake Bluff, Illinois USA) according to ASTM (E384-11 1<sup>st</sup> edition) [60]. The schematic set up of the Vickers hardness tester is shown in Figure 2.7. A load of 100 N was applied with an inverted square pyramid diamond indenter for 15s and the size of the Vickers indentation was recorded.

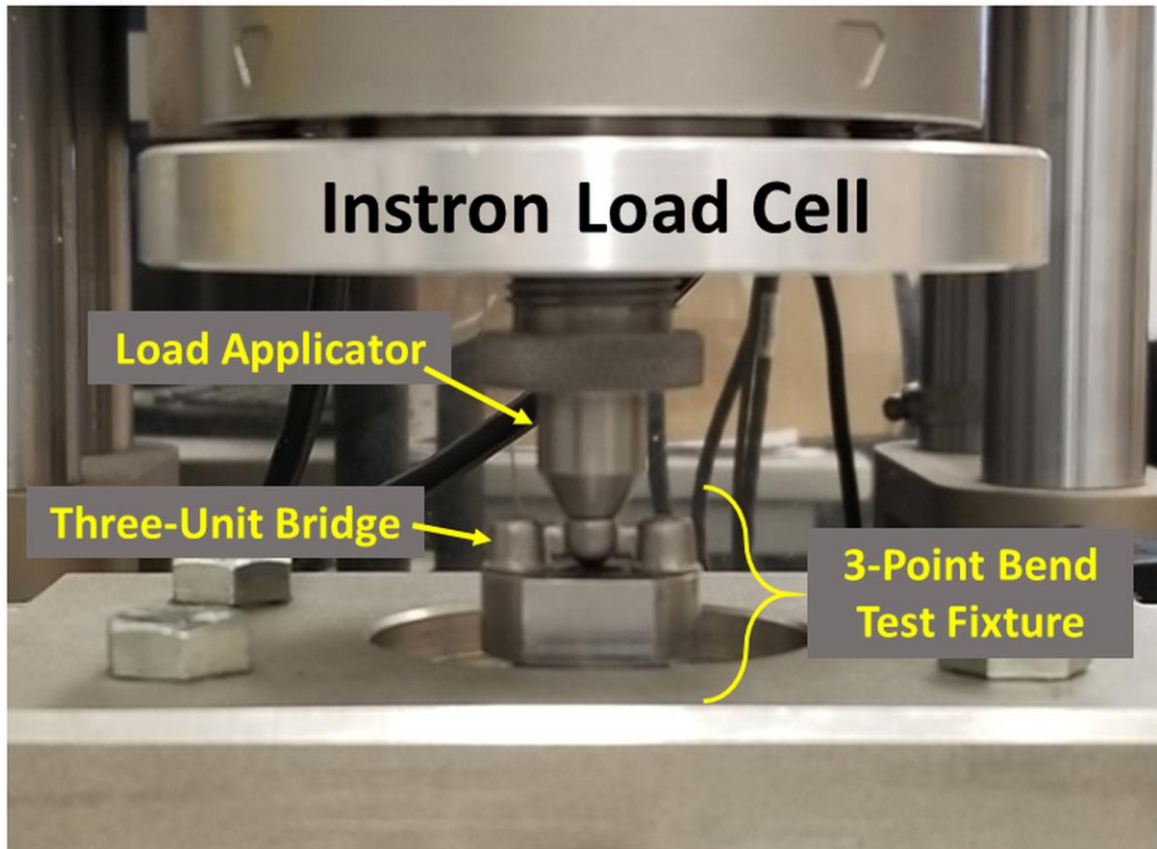


**Figure 2-5: Three-point bending test set up for the three-unit bridge Co-Cr samples**

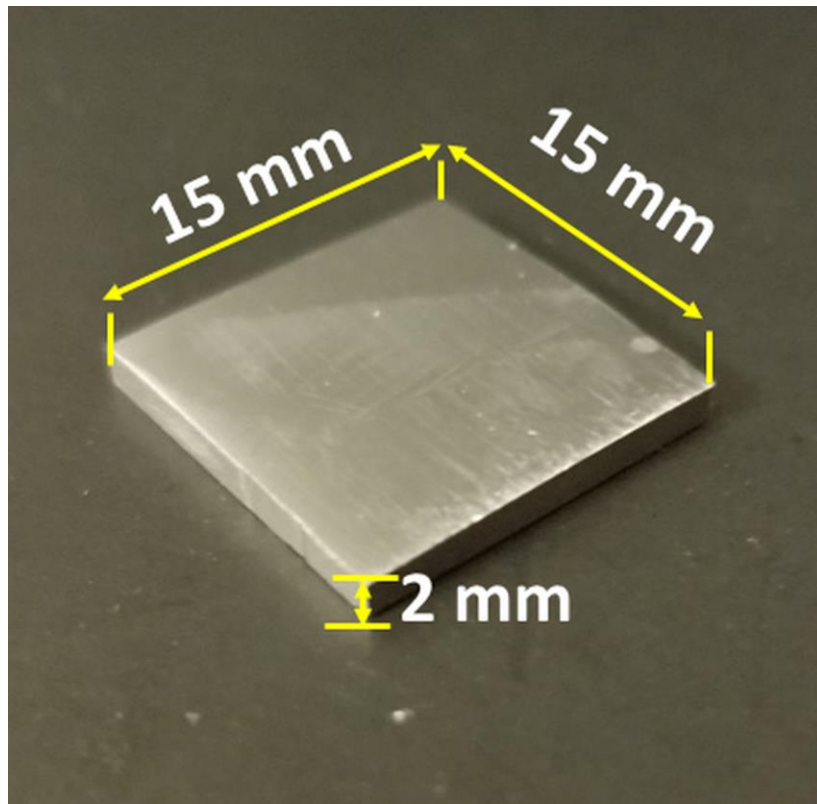


**Figure 2-6: Co-Cr square sample used for the Vickers hardness test**

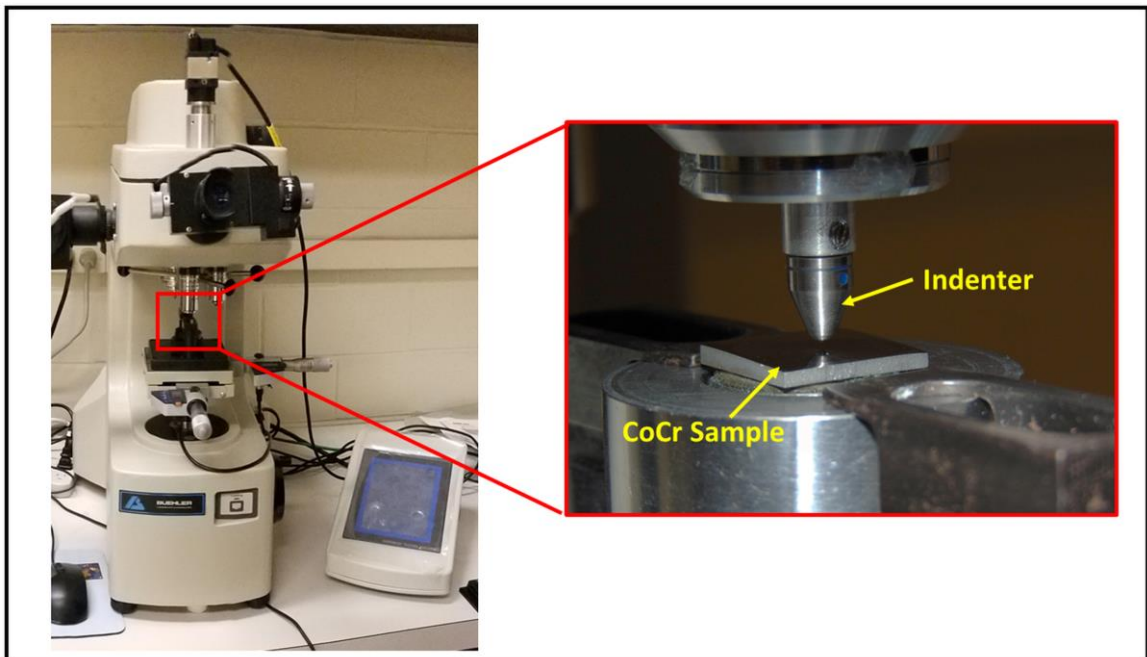


**Figure 2-7: Vickers hardness test setup for the Co-Cr square sample**

The Vickers hardness was calculated using the following equation below [60]:

$$H_v = \frac{1854.4 * P}{d^2} \quad (2)$$

Where:

$H_v$  = Hardness Vickers, (MPa)

$P$  = Force ( $g_f$ )

$d^2$  = Mean diagonal length of the indentation ( $\mu m$ )

### 2.2.3.3 Shear Bond Strength

The squared AM, milled & cast Co-Cr alloy samples (n=10) were sent to Rotsaert Laboratory (Hamilton, Ontario, Canada) for bonding of porcelain buttons (5 mm x 5mm x 2 mm) as seen in Figure 2.8.

The surfaces of all squared Co-Cr alloy samples were finished and sandblasted according to the manufacturing manual [57-59]. Then, porcelain buttons (IPS InLine® (Conventional Metal-Ceramic) were applied as specified in the literature [62]. For each group (AM, milled & cast), square samples were heat treated first before applying the porcelain layer. The procedure used for bonding the porcelain to the metal alloy substrates was done by the Rotsaert Laboratory in Hamilton, Ontario.

The shear bond strength test was performed according to ASTM (F1044-05 re-approved 2011) [63], using a universal testing machine (Instron 3345 series, INSTRON®, 825 University Ave, Norwood, MA, USA) and 5 kN load cell, at a crosshead speed of 0.5 mm/min. All specimens were sheared until fracture occurred at the interface between the porcelain and the CoCr substrate. The shear bond strength experimental set up is shown

in Figure 2.9. Based on applied forces and cross-section area parallel to the applied force, the porcelain bond strength was calculated using Equation 3.

$$\sigma_s = \frac{F}{A} \quad (3)$$

Where,

$\sigma_s$  = Shear stress (MPa)

F = Applied force (N)

A = Cross sectional area parallel to the applied force (mm<sup>2</sup>)

#### 2.2.4 Geometric Accuracy of Fabrication

The micro-CT scans of the three-unit-bridge Co-Cr previously obtained (Section 2.2.2) were reconstructed and converted from “.image file (vff)” to “.image surface file (stl)” using a MicroView 3D Image Viewer and Analysis Tool (Parallax Innovation Inc., Ilderton, ON, Canada) (see the Appendix D for details on method).

The surface file was imported into Geomagic® Qualify 12 (Geomagic, Morrisville, NC) for analysis of accuracy of fabrication for the AM, milling and casting. This was done by comparing deviations in the surfaces between the original CAD model of three-unit-bridge (reference surface) and the final fabricated structures from the different manufacturing techniques (AM, milled & cast) (test surface). The reference and test surfaces were compared to one another, to determine any discrepancy between the two surfaces (see Appendix E). This comparison involved registering the surfaces of the original three-unit bridge “.stl” as a fixed point of reference, then applying the test surface to determine the deviation between the two surface profiles.



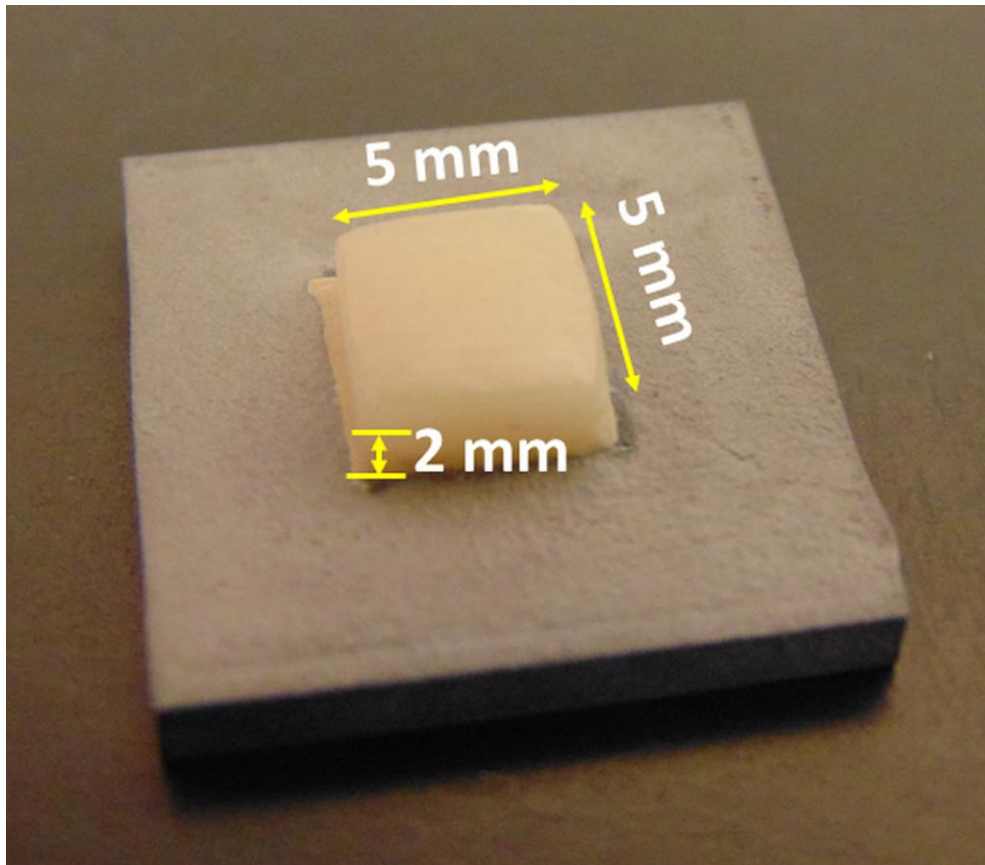


**Figure 2-8: Porcelain bonded to Co-Cr square substrate sample**

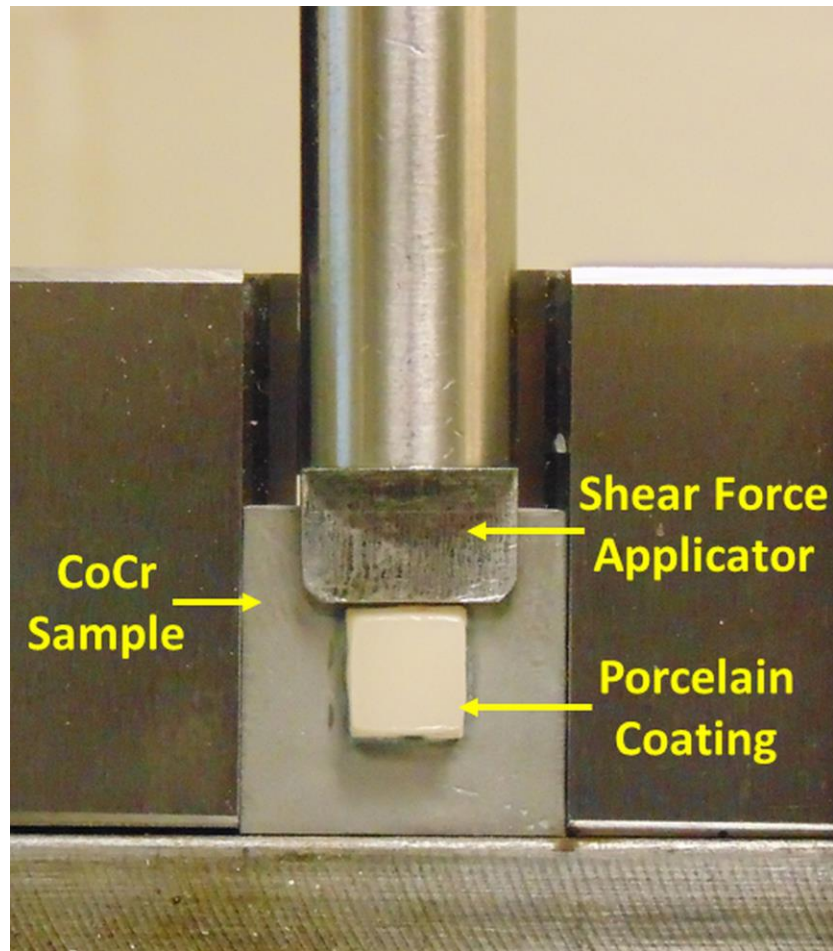


**Figure 2-9: Shear bond strength test setup**

Measurements of deviation were taken at different locations using the Sectional Based Analysis Tool in Geomagic® Qualify 12. This allowed for 2D surface deviation comparisons to be performed along two planer directions. First, the Y-Z sagittal plane was used to compare the abutment, connector, and pontic regions along the length of side-view cross section of the three-unit-bridge (Figure 2.10). Second, analysis was done along the X-Y transverse plane, which allowed comparisons of the abutment, connector, and pontic regions along the length of the top-view cross section of the three-unit-bridge (Figure 2.11).

## 2.2.5 Internal Porosity Analysis

### 2.2.5.1 Micro-CT Imaging

Micro-CT images obtained for the three-unit-bridge Co-Cr samples (AM, milled & cast) were reconstructed using the VG Studio Max 2.2 (Museum of Ontario Archaeology, London, ON, Canada), which removed any noise and corrected the grey shade scaling for the CT image.

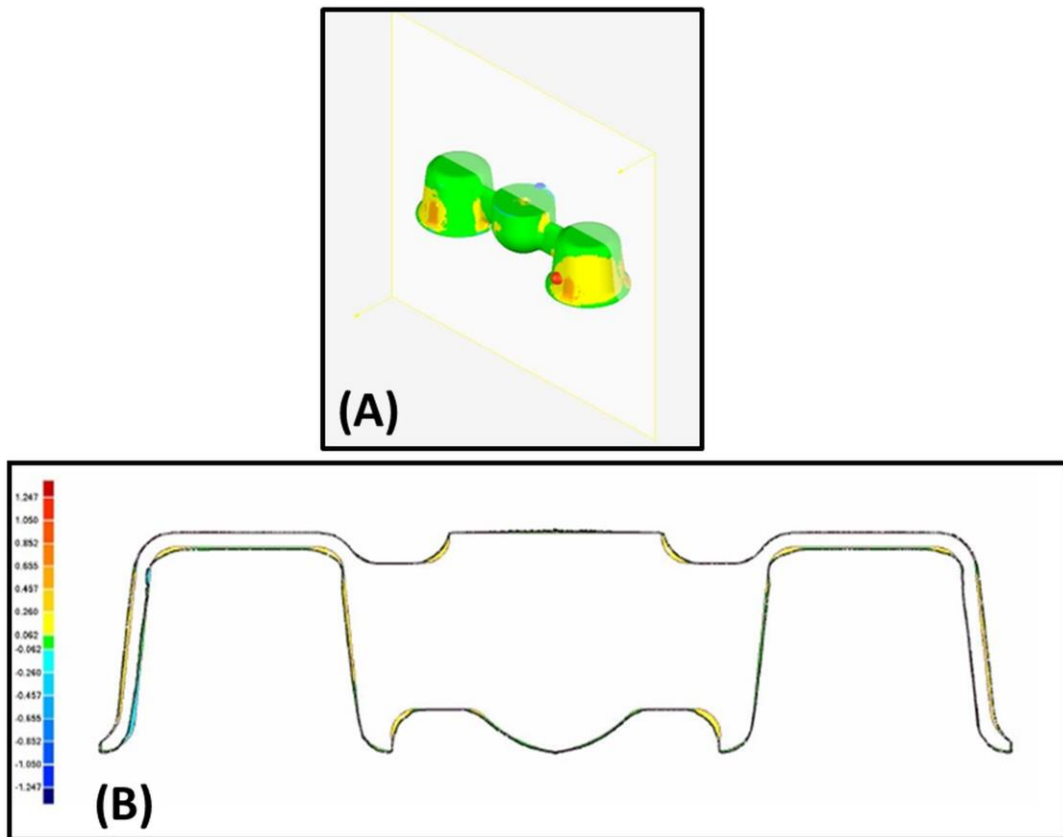


**Figure 2-10: Sagittal plane surface deviation analysis using Geomagic**

(A) The 3D color plot shows the change in the reference to the test three-unit bridge. (B) Sectional profile (Y-Z plane) shows the side-view cross-section comparing the reference (red profile) and test (black profile) surfaces

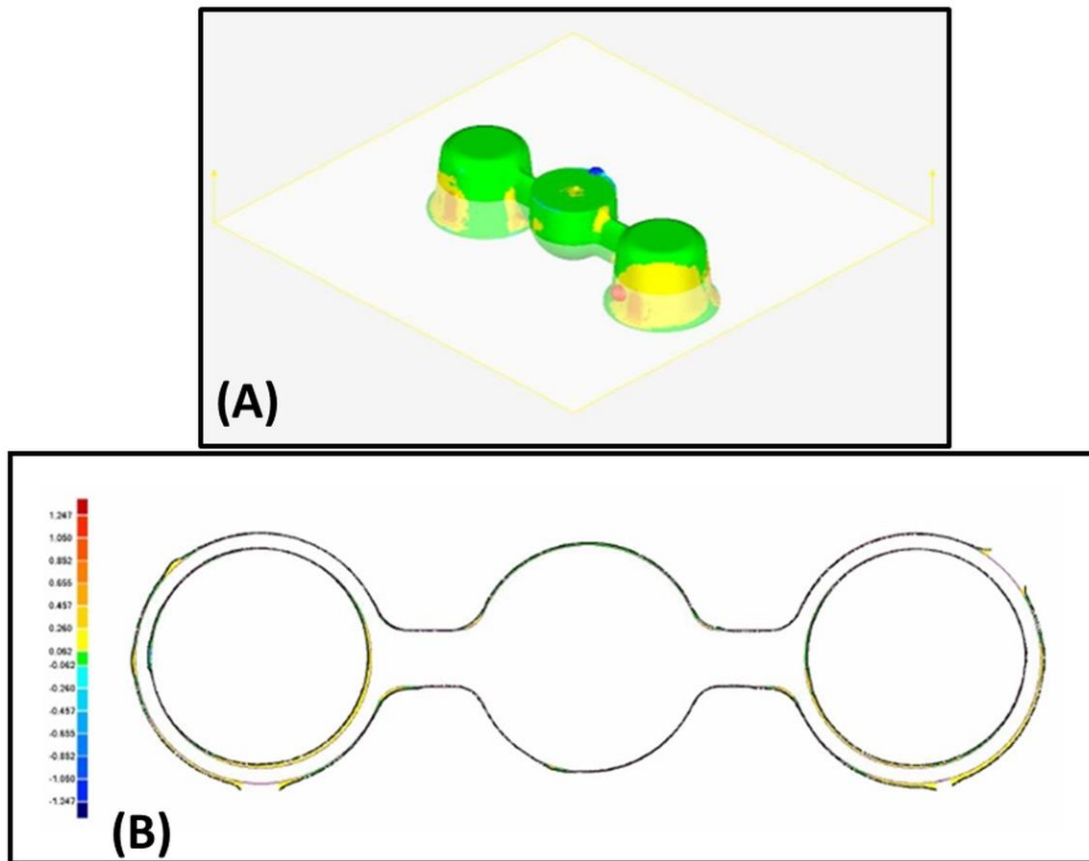


**Figure 2-11: Transverse plane surface deviation analysis using Geomagic**

(A) The 3D color plot shows the change in the reference to the test three-unit bridge. (B) Sectional profile (X-Y plane) shows the top-view cross-section comparing the reference (red profile) and test (black profile) surfaces.

### 2.2.6 Analysis of Sectioned Surfaces of Co-Cr alloys

Following bending tests, one three-unit sample from each group (AM, milled & casted) was used for optical imaging of sectioned surfaces. Each sample was sectioned at two locations along the length of the three-unit bridge (University Machine Shop, Western University, London, Ontario, Canada). Following sectioning, each sample was clamped, cold mounted in epoxy resin, and left to cure overnight.

The samples were then hand ground under water using a Buehler® Metaserv Grinding-Polisher (SR-98553) and silicon carbide Emery papers (Norton, Black Ice) at each of the grit sizes 180, 400, 600, 800, 1000, 1500, 2000 and 4000. The final polishing was conducted using colloidal silica polishing suspension solution (Master Mat TM 2, Buehler(R), 41 Waukegan Rd, Lake stuff, IL, USA).

The specimen surfaces were examined using optical microscope Nikon Digital Eclipse Camera DXM 1200 and Nikon CT-1, Version 2-20 software (Engineering Department, Western University, London, Ontario, Canada) as demonstrated in Figure 2.12.

### 2.2.7 Statistical Analysis

Statistical analysis of quantitative data was conducted using one-way analysis of variance (ANOVA) and Tukey's multiple comparative test at 95% level of confidence (Graph Pad Prism 6, GraphPad Software, San Diego, CA).

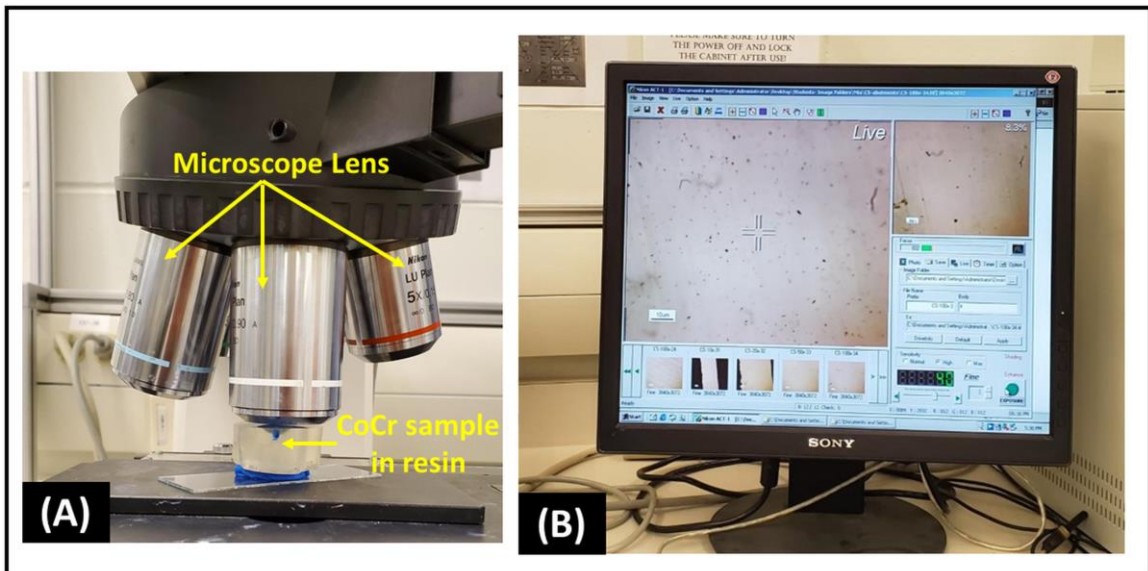


**Figure 2-12: Optical Microscope Image setup using the Nikon Digital Eclipse Camera DXM 1200 and Nikon ACT-1, Version 2-20 software**

(A) Co-Cr sample setup and the orientation under the objective. (B) software image display.

## Chapter 3

### 3 Results

#### 3.1 Overview

This chapter describes the properties of metal structures made using AM technology as compared to those made using the conventional methods of casting and milling. The following properties were evaluated: bending strength and load at fracture, hardness, porcelain adherence, accuracy of fabrication, and internal porosity.

#### 3.2 Mechanical Properties of the Rectangular Bar Specimens

##### 3.2.1 Three Point Bend Test for Rectangular Bar Specimens

When comparing flexural strength, AM specimens exhibited greatest maximum flexural stress ( $2219 \pm 14$  MPa) and load at fracture ( $2.696 \pm 0.010$  kN) under three-point bending ( $p < 0.05$ ), with cast samples withstanding significantly higher stresses ( $1489 \pm 38$  MPa) and loads at fracture ( $1.95 \pm 0.03$  kN) compared to milled samples (stress:  $1057 \pm 23$  MPa; load at fracture:  $1.42 \pm 0.03$  kN) ( $p < 0.05$ ). Despite these significant differences in flexural strength, the flexural modulus values of AM ( $131.94 \pm 1.88$  MPa), milled ( $128.17 \pm 0.80$  MPa), and cast ( $125.23 \pm 4.69$  MPa) samples were not significantly different ( $p > 0.05$ ) as shown in the Figure 3.1. Flexural stress and load are both indicative of the forces required for material failure, while flexural modulus indicates the stiffness or tendency of the material to deform prior to failure.

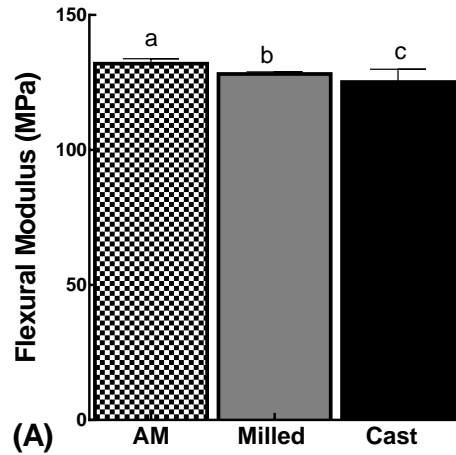


### 3.2.2 Vickers Hardness for Bar Samples

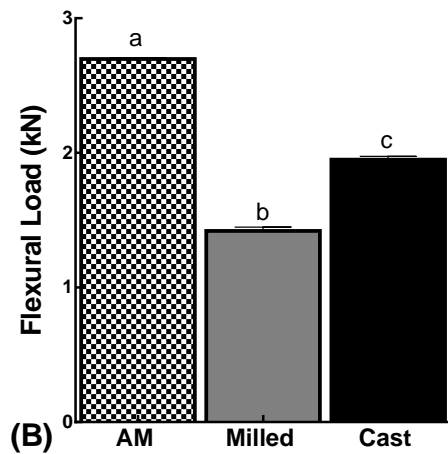
Vickers hardness measures the sample's resistance to localized deformation due to a constant force load applied from a sharp object. Vickers hardness data indicated that samples fabricated by AM exhibited significantly greater hardness ( $490.17 \pm 2.58$  MPa) compared to milled or cast samples ( $p < 0.05$ ). Between milling and casting, the cast samples showed significantly greater hardness ( $406.44 \pm 3.36$  MPa) than the milled samples ( $337.01 \pm 3.11$  MPa) ( $p < 0.05$ ) (Figure 3.2).

### 3.2.3 Shear Bond Strength for Bar Samples

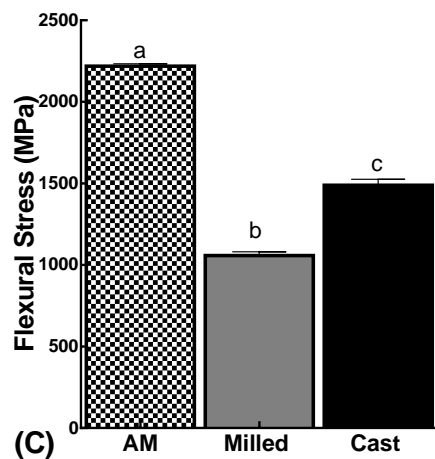
Shear bond strength defines the maximum stress required to detach the porcelain coating layer from the metal surface. Overall, AM ( $31.50 \pm 2.15$  MPa) and milled ( $30.79 \pm 2.78$  MPa) samples demonstrated significantly greater shear bond strength compared to a cast samples ( $24.87 \pm 1.094$  MPa) ( $p < 0.05$ ), with no significant differences found between AM and milled samples ( $p > 0.05$ ) (Figure 3.3).



(A)



(B)



(C)

**Figure 3-1: Mechanical properties of Co-Cr alloy bar samples fabricated by AM, milling or casting**

Data are mean values of flexural modulus (A), flexural load (B) and flexural stress (C) for AM, milled and cast samples. Error bars represent the standard error of the mean (SEM), n=15 samples for each group. The same lowercase letters indicate no significant differences between groups ( $p>0.05$ ).

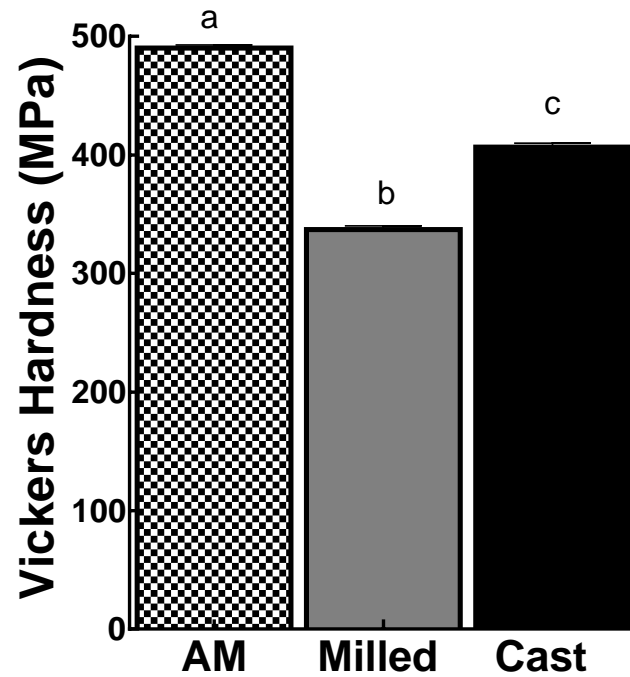


**Figure 3-2: Vickers Hardness of Co-Cr alloy bar samples fabricated by AM, milling or casting**

Data are means  $\pm$  SEM, n= 10 samples for each group. Significant differences ( $p < 0.05$ ) were observed among AM, milled and cast samples as indicated by different lowercase letters.

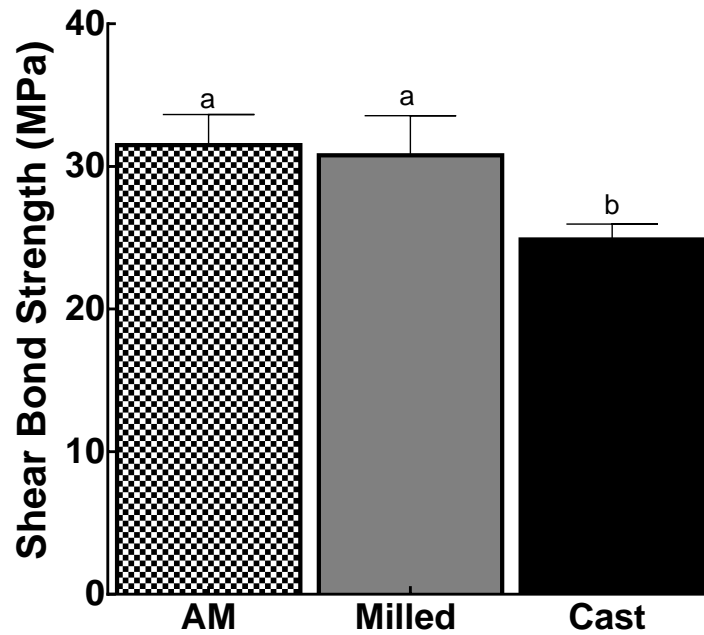


**Figure 3-3: Shear bond strength of porcelain coating on Co-Cr alloy specimens made by AM, milling or casting**

Data are means  $\pm$  SEM, n= 10 samples for each group. The same lowercase letters indicate no significant differences between groups ( $p>0.05$ ).

### 3.3 Mechanical Properties of Three-Unit Bridges

#### 3.3.1 Three Point Bend Test for Three-Unit Bridge samples

When comparing loads at failure, three-unit bridge substructures fabricated using AM showed similar flexural loads at failure ( $5.78 \pm 0.062$  kN) compared to milled ( $5.71 \pm 0.12$  kN) and cast ( $6.27 \pm 0.16$  kN) samples ( $p > 0.05$ ). While comparing the flexural stiffness of the materials prior to failure, AM ( $5.77 \pm 0.12$  kN/mm) and cast ( $5.91 \pm 0.11$  kN/mm) substructures showed significantly greater stiffness than milled samples ( $4.68 \pm 0.25$  kN/mm) ( $p < 0.05$ ). However, no significant differences were found between the AM and Cast samples ( $p > 0.05$ ) (Figure 3.4).

### 3.4 Internal Porosity Analyses

#### 3.4.1 Porosity Assessment using Micro-CT Imaging

Based on qualitative assessment of micro-CT images, AM samples consistently showed porosity in the abutment region of the three-unit bridges, compared to milled and cast substructures. In comparison, random distributions of small voids were observed only in the connector and pontic regions of AM and cast substructures (Figure 3.5). No voids were apparent in the milled samples.

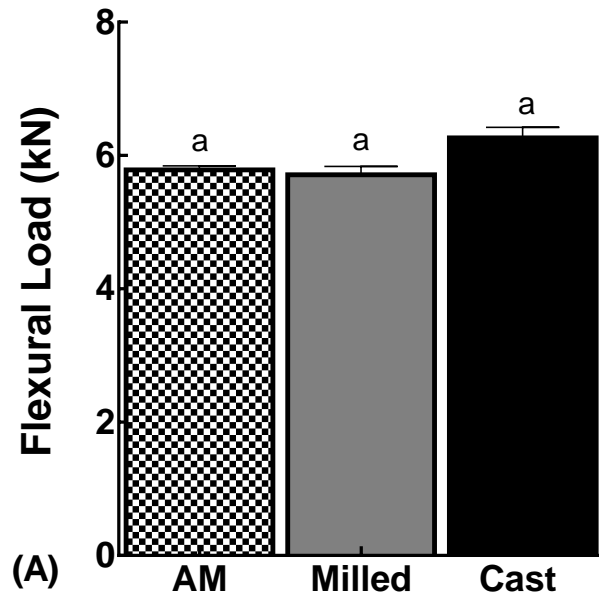
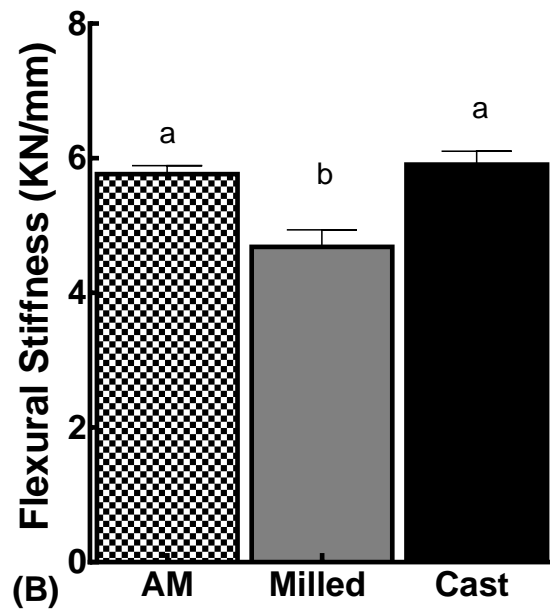


**Figure 3-4: Mechanical properties of Co-Cr three-unit bridge substructures fabricated by AM, milling or casting**



Data are means  $\pm$  SEM,  $n = 9$  samples for each group. The same lowercase letters indicate no significant differences between groups ( $p > 0.05$ ).

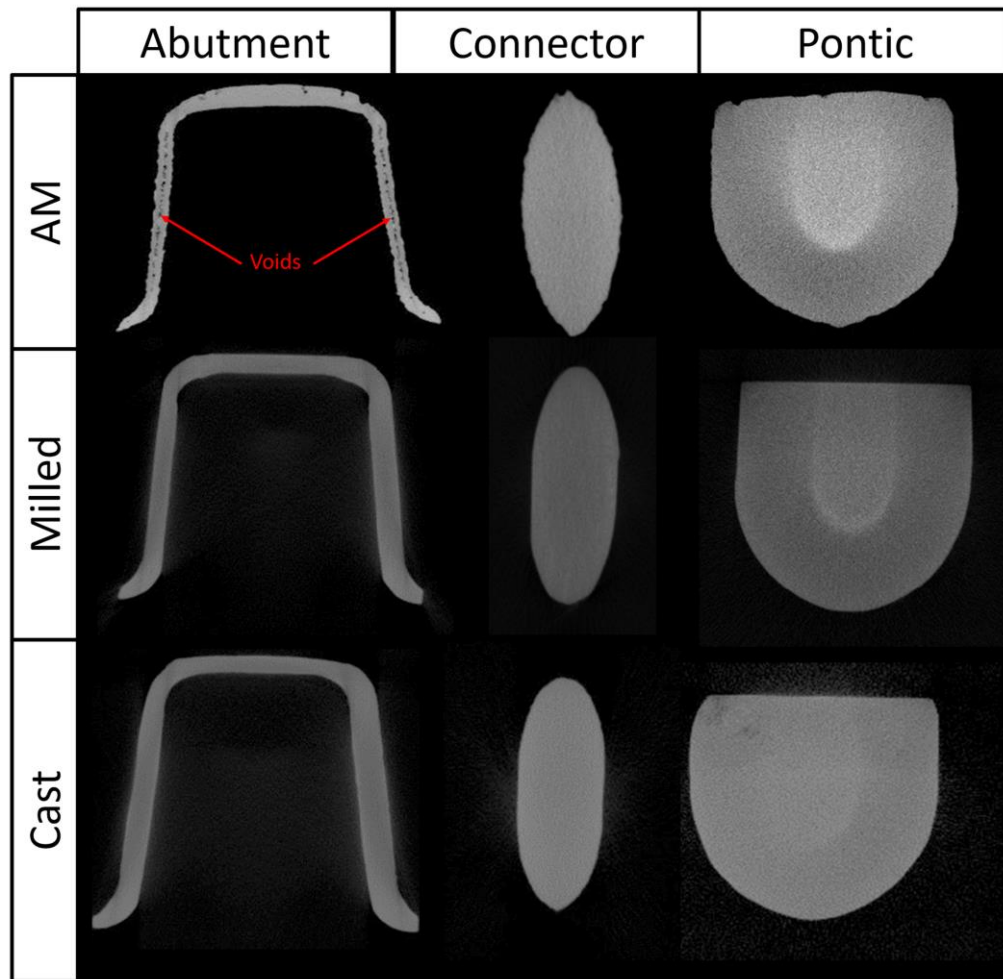


**Figure 3-5: Representative cross-sectional micro-CT images of AM, milled and cast three-unit bridges**

The red arrows indicate the voids within the abutment region of the AM substructure.

### 3.4.2 Porosity Assessment using Optical Imaging

Qualitative analysis of porosity from optical imaging showed porosity in the abutment region of the AM sample, consistent with that observed from micro-CT imaging (Figure 3.6). Voids were observed in the abutment regions of the milled and cast substructures, but these were smaller and fewer than that observed with AM. When comparing porosity in the connector regions (Figure 3.7), all the three groups showed voids. However, cast samples exhibited larger and greater numbers of voids within the connector compared to AM and milled samples.

## 3.5 Geometric Accuracy of Fabrication

The original CAD model of the three-unit bridge design and micro-CT surface models for AM, milled and cast substructures were compared. Results showed that all micro-CT models (AM, milled and cast) exhibited surface deviations within 12 micrometers from the ideal CAD model. There were no significant differences among the AM ( $9.03 \pm 1.13 \mu\text{m}$  &  $10.26 \pm 1.57 \mu\text{m}$ ), milled ( $6.73 \pm 0.29 \mu\text{m}$  &  $8.76 \pm 1.33 \mu\text{m}$ ) and cast ( $5.80 \pm 1.71 \mu\text{m}$  &  $5.51 \pm 0.99 \mu\text{m}$ ) sample for surface deviations in YZ and XY planes, respectively ( $p > 0.05$ ) (Figure 3.8).



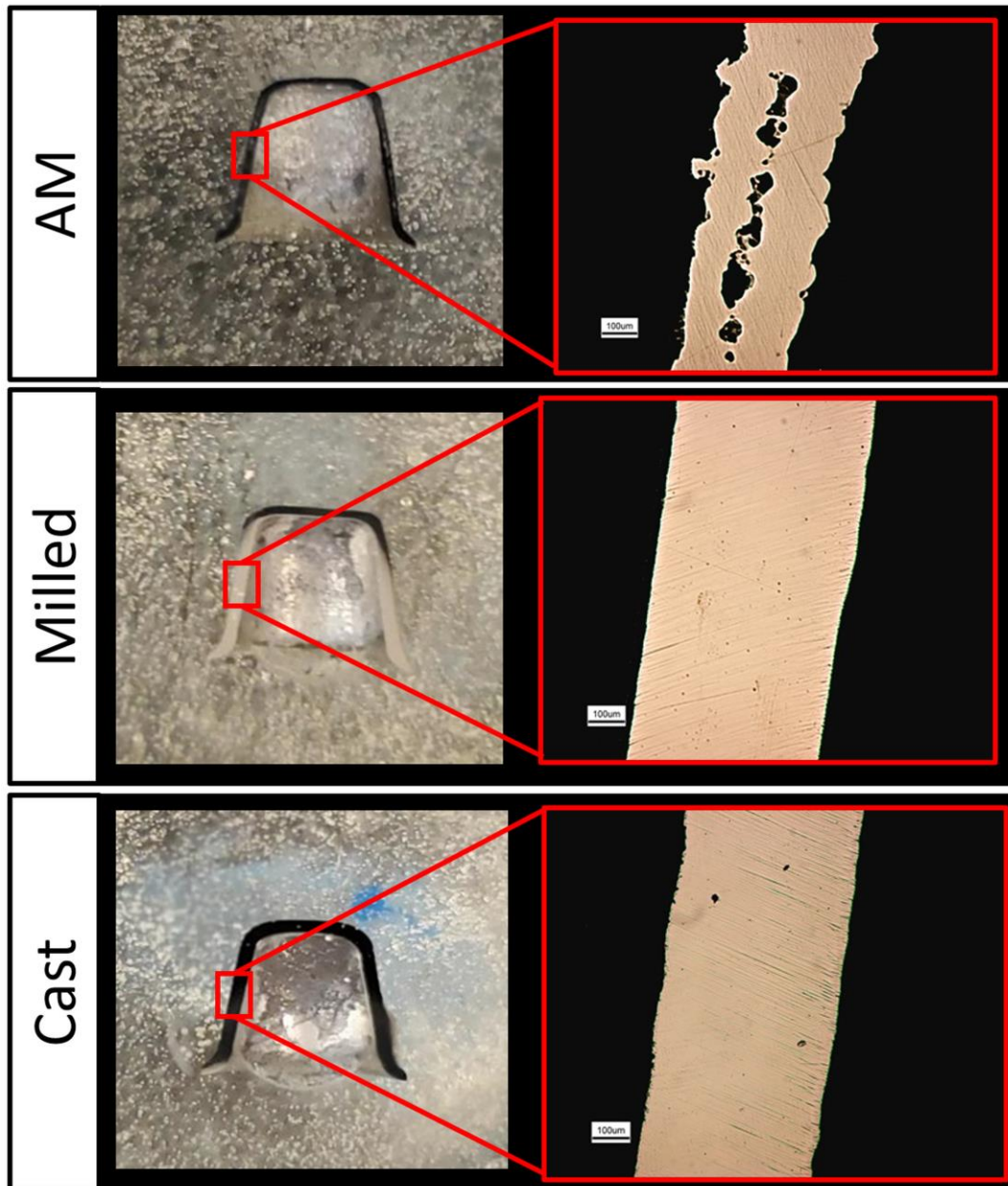


**Figure 3-6: Optical images of the abutment for AM, milled and cast three-unit bridge substructures**

Magnified regions within the abutments are shown at right (scale bars are 100 µm).

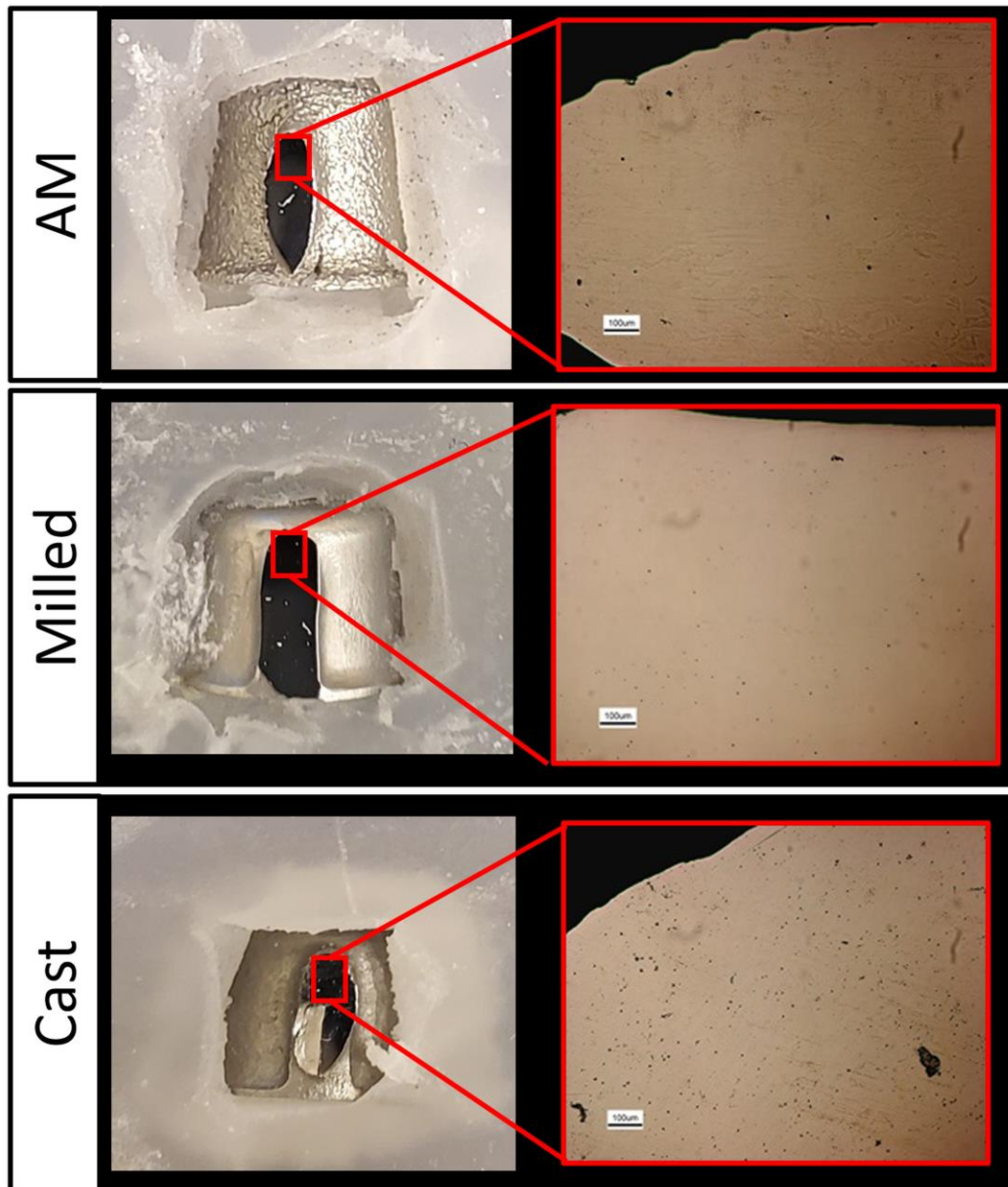


**Figure 3-7: Optical images of the connector for the AM, milled and cast three-unit bridge substructures**

Magnified regions within the abutments are shown at right (scale bars are 100 µm).

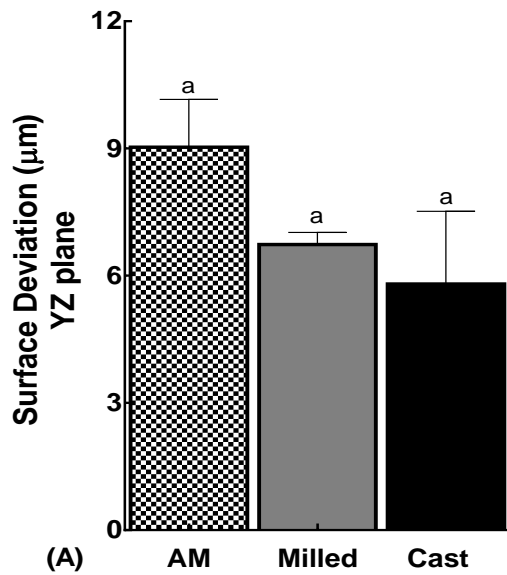
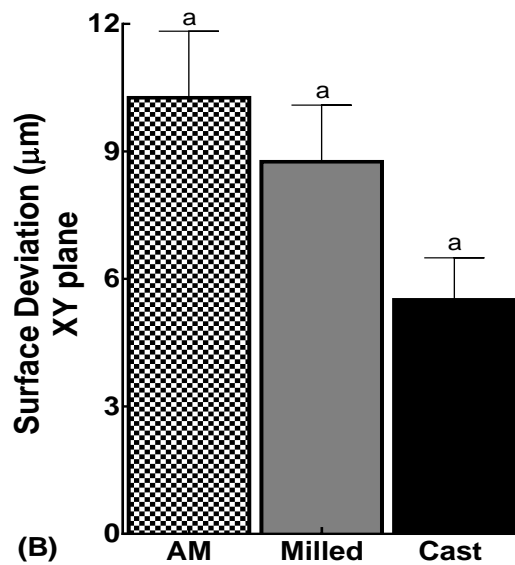


**Figure 3-8: Accuracy of fabrication of three-unit bridge substructures produced by AM, milling or casting.**



The original CAD model of the three-unit bridge design and micro-CT surface models for AM, milled and cast substructures were compared. (A) Surface deviation in the YZ plane, and (B) Surface deviation in the XY plane ( $\mu\text{m}$ ). Data are means  $\pm$  SEM,  $n = 5$  samples for each group. The same lowercase letters indicate no significant difference between groups ( $p > 0.05$ ).

## Chapter 4

### 4.1 Discussion

Among the different techniques of fabrication for dental Co-Cr restorations, AM continues to show promise in its ability to meet the limitations of conventional manufacturing. These include shape and functional complexity, time efficiency and less manual labor, less waste and impact on environments, and design alteration. However, within the Canadian dental manufacturing industry, its application has not been widely adopted, as compared to other international industries [9], [64], [65]. The reason for this could be due to lack of the literature regarding the performance of AM technology for the fabrication dental devices. It is necessary to explore metal AM compared to conventional manufacturing methods in order to demonstrate and show its potential success for dental device fabrication in Canada. The studies described in this thesis addressed the lack of information in the literature regarding the performance of AM fabricated restorations compared to conventionally manufactured ones.

Overall, the findings from this thesis show promise for AM as a potential method for the fabrication of dental devices, when compared to conventional manufacturing. As shown, dental specimens fabricated using AM technology performed equivalent to or better than samples fabricated using conventional manufacturing, based on results from mechanical testing. When comparing quantitative and qualitative results from porosity analysis, AM samples showed similar or superior results to samples produced by milling or casting. No significant differences in accuracy of fabrication were found among the AM,

milled and cast samples, where all deviations were within 12 micrometers from the ideal CAD model.

The differences in the mechanical properties and behavior among the rectangular bar specimens and three-unit bridge substructures fabricated by AM, milling and casting provided information regarding their potential clinical performance. Three-point bend tests were used to assess the mechanical properties of the Co-Cr alloys from the three different fabrication methods (AM, milling, casting). Three-point bending was meant to simulate the most common loading mechanism expected for FPDs, bending under the forces of mastication. Bend tests were performed on sample rectangular bars designed from (ASTM-E290-97a) standards, to report on the bending properties specific to alloy compositions used with the various fabrication methods. These results provided data associated with standardized reporting on the flexural properties of alloys. Based on the results of mechanical properties, the AM specimens showed greater flexural load and stress at fracture compared with the cast and milled samples. Among the three groups, similar flexural modulus was found. These results indicate that AM specimens showed greatest strength in resisting fracture compared to milled and cast samples. However, all three samples (AM, mill, cast) showed similar stiffness for the duration of loading.

Additionally, bend testing was performed on three-unit bridges fabricated by AM, milling and casting, to provide stress-strain data for designs that were clinically relevant for dental applications. When comparing the results of three-point bending for the three-unit bridges, it was observed that fracture occurred at the level of the connector region. The connectors appeared to deform, followed by crack propagation, resulting in eventual fracture of the specimen. AM, cast and milled samples showed similar flexural loads at

failure. However, AM and cast showed higher flexural stiffness compared to milled samples.

These results of three-point bend testing were different from that found by Øilo et al. [40]. In their study, three-unit bridges were fabricated with AM, casting and milling, but fracture of the connectors were not observed. However, there was severe deformation in the walls of the crown, followed by ruptures along the occlusal surface from the crown margin [40]. As well, in their study, AM exhibited the highest stiffness compared to samples prepared by casting or milling [40]. Similarly, Han et al. stated that AM was superior to conventional techniques of manufacturing fixed dental restorations [65], while Wu et al. stated that the yield and tensile strengths of the AM were statistically higher than the cast alloy [66].

Vickers hardness is a test that measures the ability of the alloy to resist the local permanent deformation. In this thesis, AM samples exhibited the highest resistance to deformation compared to the milled and cast samples. Similar results were found in the study by Han et. al., where AM samples were harder compared to the cast and milled samples. Øilo et al. also reported that the AM method performed better in hardness testing than milled and cast [40].

Shear bond strength testing evaluated the strength of the porcelain bond with the metal interface for AM, cast and milled samples. According to the International Standard for metal-ceramic systems in dentistry (ISO 9693:2012), the minimum acceptable bond strength is 25 MPa [67]. The mean bond strength values found in this thesis for samples prepared from AM, cast and milled Co-Cr alloys all exceeded the minimum values defined

in ISO 9693:2012. In this study, AM and milled exhibited the highest bond strength compared to cast samples. Similar results were found by Ekren et. al. when comparing selective laser melting and selective laser sintering AM technologies, reporting average bond strength values in excess of the minimum requirements of ISO 9693:2012 [45]. Similarly, Ren et. al. showed that AM exceeded the minimum value, which gives an indication that AM fabrication is an acceptable technique for metal-ceramic bond strength in a clinical application [68].

Based on the micro-CT and optical imaging analyses of internal porosity, the AM specimens showed consistent distribution of large voids within the walls of the abutment of the three-unit bridge, while the milled and cast had fewer and smaller voids in the abutment region. The reason for the voids within the internal surface of the AM abutments is probably due to the AM laser process parameters for the thin wall section. The laser beam may not have appropriately melted the Co-Cr powder particles adjacent to the center of the structures [39]-[62].

The contradiction of the qualitative porosity results may be due to the definition of voids in the micro-CT images. The voids observed during qualitative analysis (*i.e.*, visual inspection of optical images) may not have a greyscale value equivalent to that of air, and therefore was not identified and quantified in the micro-CT analyses. As well, the size of the voids relative to the resolution of the micro-CT system may have affected the detection of a micro-void for the future quantitative assessments.

The presence of internal porosity within the AM and cast three-unit bridges did not have a negative effect on the mechanical performance of the substructures. AM and cast

three-unit bridges showed similar flexural loads at fracture, and greater flexural stiffness, compared to the milled equivalents. Similarly, Wits et. al. investigated the porosity of AM parts by focusing on the capability to produce a near full dense part, and validated it using two techniques of measuring porosity: CT and microscopic images [53]. They found that the non-uniformity of pore distributions did not affect the tensile testing results from the metal-based AM technology [53]. Future studies will aim to investigate the effect of porosities on the fatigue properties of AM samples, since microstructure is not only related to strength, stiffness, and hardness, but generally also important to fatigue behavior.

When the CAD model of the three-unit bridge design and micro-CT model for the AM, milled and cast substructures were compared to determine the accuracy of fabrication, no significant differences were found among the AM, milled and cast samples for surface deviations in XY and YZ planes. This thesis reported the accuracy of fabrication, which is a comparison of the final fabricated three-unit bridge geometry relative to the original CAD design. This measure was used to determine how well the final fabricated structure met the specifications of the design. All final fabrications (AM, milled and cast) were within 12 micrometers of the CAD model design.

A better clinical measure of final fabrication geometry would be marginal fit. Marginal fit quantifies the marginal seal at the tooth-crown interface. It is an important factor for the prevention of recurrent caries, periodontal diseases and longevity of the restoration [69]. *In vivo* studies have shown correlation between the marginal fit and the plaque accumulation; larger marginal discrepancy led to microalgae's and periodontal inflammation around the restoration [70]. Such a measure was assessed by Zuskova et. al., where overall fit was compared between milled and AM technology. On average, milled



samples were shown to have a better overall fit compared to the AM group [71]. Future studies will aim to assess marginal fit of AM samples relative to those fabricated by the conventional methods of dental manufacturing.

## 4.2 Conclusions

Within the limitations of this *in vitro* study, the following conclusions were drawn:

1. For the rectangular Co-Cr bar samples, it was determined:
  - a. AM samples showed significantly higher flexural stress and hardness compared to the milled and cast equivalents.
  - b. AM samples exhibited slightly higher flexural modulus than cast and milled samples.
  - c. AM and milled samples showed greater shear bond strength compared to cast equivalents. All bond strength values (AM, milled, cast) were greater than 25 MPa, which is critical for the metal-ceramic interface bond, as determined by ISO standards for the dental materials.
2. For a clinically representative Co-Cr three-unit bridge design, it was determined:
  - a. AM, milled and cast samples showed similar flexural loads at fracture.
  - b. AM and cast samples showed greater flexural stiffness compared to milled equivalents.

3. Based on the qualitative assessment of internal porosity within the three-unit bridge samples, it was determined:
  - a. AM samples showed consistent voids along the abutment region of the three-unit bridge compared to the cast and milled samples.

Overall, the clinical implication for Co-Cr dental frameworks or substructures fabricated by AM technology is promising and comparable to those manufactured by conventional casting or milling.

## References

- [1] S. H. Huang, P. Liu, A. Mokasdar, and L. Hou, "Additive manufacturing and its societal impact: A literature review," *Int. J. Adv. Manuf. Technol.*, vol. 67, no. 5–8, pp. 1191–1203, 2013.
- [2] R. A. of Engineering, "Additive manufacturing : opportunities and constraints," *A Summ. a roundtable forum held 23 May 2013*, no. May 2013, 2013.
- [3] E. Herderick, "Additive manufacturing of metals: A review," *Mater. Sci. Technol. Conf. Exhib. 2011*, vol. 2, no. 176252, pp. 1413–1425, 2011.
- [4] T. M. A. Kohli, "3D Printing in Dentistry-An Overview," *Acta Sci. Dent. Sci.*, vol. 3, no. 6, pp. 35–41, 2019.
- [5] S. N. Kurenov, C. Ionita, D. Sammons, and T. L. Demmy, "Three-dimensional printing to facilitate anatomic study, device development, simulation, and planning in thoracic surgery," *J. Thorac. Cardiovasc. Surg.*, vol. 149, no. 4, pp. 973-979.e1, 2015.
- [6] D. I. Wimpenny, P. M. Pandey, and L. Jyothish Kumar, "Advances in 3D Printing & additive manufacturing technologies," *Adv. 3D Print. Addit. Manuf. Technol.*, pp. 1–186, 2016.
- [7] R. Van Noort, "The future of dental devices is digital," *Dent. Mater.*, vol. 28, no. 1, pp. 3–12, 2012.
- [8] X. W. Ren, L. Zeng, Z. M. Wei, X. Z. Xin, and B. Wei, "Effects of multiple firings on metal-ceramic bond strength of Co-Cr alloy fabricated by selective laser

- melting,” *J. Prosthet. Dent.*, vol. 115, no. 1, pp. 109–114, 2016.
- [9] N. Xiang, X. Z. Xin, J. Chen, and B. Wei, “Metal-ceramic bond strength of Co-Cr alloy fabricated by selective laser melting,” *J. Dent.*, vol. 40, no. 6, pp. 453–457, 2012.
- [10] L. Zeng, Y. Zhang, Z. Liu, and B. Wei, “Effects of repeated firing on the marginal accuracy of Co-Cr copings fabricated by selective laser melting,” *J. Prosthet. Dent.*, vol. 113, no. 2, pp. 135–139, 2015.
- [11] L. Wu, H. Zhu, X. Gai, and Y. Wang, “Evaluation of the mechanical properties and porcelain bond strength of cobalt-chromium dental alloy fabricated by selective laser melting,” *J. Prosthet. Dent.*, vol. 111, no. 1, pp. 51–55, 2014.
- [12] A. Barazanchi, K. C. Li, B. Al-Amleh, K. Lyons, and J. N. Waddell, “Additive Technology: Update on Current Materials and Applications in Dentistry,” *J. Prosthodont.*, vol. 26, no. 2, pp. 156–163, Feb. 2017.
- [13] Y. P. Kathuria, “Microstructuring by selective laser sintering of metallic powder,” *Surf. Coatings Technol.*, vol. 116–119, pp. 643–647, 1999.
- [14] A. Bhargav, V. Sanjairaj, V. Rosa, L. W. Feng, and J. F. Yh, “Review Article Applications of additive manufacturing in dentistry: A review,” pp. 2058–2064, 2017.
- [15] Y. Zhou, N. Li, J. Yan, and Q. Zeng, “Comparative analysis of the microstructures and mechanical properties of Co-Cr dental alloys fabricated by different methods,” *J. Prosthet. Dent.*, vol. 120, no. 4, pp. 617–623, 2018.
- [16] A. Azari and S. Nikzad, “The evolution of rapid prototyping in dentistry: A review,”

*Rapid Prototyp. J.*, vol. 15, no. 3, pp. 216–225, 2009.

- [17] “3D Printing of Metals A Thesis Presented by Ying Mu to The Graduate School in Partial Fulfillment of the Requirements for the Degree of Master of Science in Materials Science and Engineering Stony Brook University August 2016,” no. August, 2016.
- [18] C. F. Driscoll *et al.*, “The Glossary of Prosthodontic Terms,” *J. Prosthet. Dent.*, vol. 117, no. 5, pp. C1-e105, 2017.
- [19] J. Zhao and X. Wang, “Dental Prostheses,” *Adv. Ceram. Dent.*, pp. 23–49, 2014.
- [20] M. H. R. Subhashini, G. Abirami, and A. R. Jain, “Abutment selection in fixed partial denture - A review,” *Drug Invent. Today*, vol. 10, no. 1, 2018.
- [21] N. Kaleli and D. Saraç, “Comparison of porcelain bond strength of different metal frameworks prepared by using conventional and recently introduced fabrication methods,” *J. Prosthet. Dent.*, vol. 118, no. 1, pp. 76–82, 2017.
- [22] H. Wang, Q. Feng, N. Li, and S. Xu, “Evaluation of metal-ceramic bond characteristics of three dental Co-Cr alloys prepared with different fabrication techniques,” *J. Prosthet. Dent.*, vol. 116, no. 6, pp. 916–923, 2016.
- [23] D. A. Widyasrini, *Dental Materials Foundations and Applications*, vol. 8, no. 1. 2019.
- [24] Kenneth Anusavice Chiayi Shen H. Ralph Rawls, *Philips Science of Dental Materials*, 12th editi. Elsevier, 2012.
- [25] Ronald L. Sakaguchi and John M. Powers, *Restorative dental materials, ed. 7*, 13th

editi. Elsevier Mosby, 2006.

- [26] M. S. Spiller, H. Science, and E. Megan, “Castable Metal Alloys in Dentistry,” 2020.
- [27] Nasruddin, M.F. 2015. Accuracy of Computer-Aided Design/Computer- Assisted Manufacture (CAD/CAM) Fabricated Dental Restorations: A comparative study. PhD Thesis, University College Cork.
- [28] L. Hian, “Dental ceramics : a review of new materials and processing methods Monolithic zirconia restorations,” vol. 31, pp. 133–146, 2017.
- [29] T. Miyazaki and Y. Hotta, “CAD / CAM systems available for the fabrication of crown and bridge restorations,” pp. 97–106, 2011.
- [30] C. A. D. Cam-generated and C. A. D. Cam, “The clinical performance of CAD/CAM-generated composite inlays,” *J. Am. Dent. Assoc.*, vol. 136, no. 12, pp. 1714–1723, 2005.
- [31] V. Gulati, “Advancement of CAD / CAM in Prosthetic Dentistry : A Review,” vol. 3, no. 7, pp. 491–495, 2016.
- [32] G. Bosch, A. Ender, and A. Mehl, “A 3-dimensional accuracy analysis of chairside CAD / CAM milling processes,” *J. Prosthet. Dent.*, vol. 112, no. 6, pp. 1425–1431.
- [33] Y. Tomita, J. Uechi, M. Konno, S. Sasamoto, M. Iijima, and I. Mizoguchi, “Accuracy of digital models generated by conventional impression / plaster-model methods and intraoral scanning,” vol. 37, no. 4, pp. 628–633, 2018.
- [34] O. Alageel, M. N. Abdallah, A. Alsheghri, J. Song, E. Caron, and F. Tamimi, “Removable partial denture alloys processed by laser-sintering technique,” *J.*

- Biomed. Mater. Res. - Part B Appl. Biomater.*, vol. 106, no. 3, pp. 1174–1185, 2018.
- [35] H. Chen, H. Li, Y. Zhao, X. Zhang, Y. Wang, and P. Lyu, “Adaptation of removable partial denture frameworks fabricated by selective laser melting,” *J. Prosthet. Dent.*, vol. 122, no. 3, pp. 316–324, 2019.
- [36] M. Revilla-león and M. Özcan, “Additive Manufacturing Technologies Used for 3D Metal Printing in Dentistry,” pp. 201–208, 2017.
- [37] D. Herzog, V. Seyda, E. Wycisk, and C. Emmelmann, “Additive manufacturing of metals,” *Acta Mater.*, vol. 117, pp. 371–392, 2016.
- [38] T. Koutsoukis, S. Zinelis, G. Eliades, K. Al-wazzan, M. Al Rifaiy, and Y. S. Al Jabbari, “Selective Laser Melting Technique of Co-Cr Dental Alloys : A Review of Structure and Properties and Comparative Analysis with Other Available Techniques,” vol. 24, pp. 303–312, 2015.
- [39] K. V. Venkatesh and V. V. Nandini, “Direct Metal Laser Sintering : A Digitised Metal Casting Technology,” vol. 13, no. 4, pp. 389–392, 2013.
- [40] M. Øilo, H. Nesse, O. J. Lundberg, and N. R. Gjerdet, “Mechanical properties of cobalt-chromium 3-unit fixed dental prostheses fabricated by casting, milling, and additive manufacturing,” *J. Prosthet. Dent.*, vol. 120, no. 1, pp. 156.e1-156.e7, 2018.
- [41] C. Y. Yap *et al.*, “Review of selective laser melting: Materials and applications,” *Appl. Phys. Rev.*, vol. 2, no. 4, 2015.
- [42] P. K. Gokuldoss, S. Kolla, and J. Eckert, “Additive manufacturing processes: Selective laser melting, electron beam melting and binder jetting-selection guidelines,” *Materials (Basel)*, vol. 10, no. 6, 2017.

- [43] K. G. Prashanth, S. Scudino, and J. Eckert, "Defining the tensile properties of Al-12Si parts produced by selective laser melting," *Acta Mater.*, vol. 126, pp. 25–35, 2017.
- [44] J. C. Wataha, "Alloys for prosthodontic restorations," vol. 1975, pp. 351–363, 2002.
- [45] O. Ekren, A. Ozkomur, and Y. Ucar, "Effect of layered manufacturing techniques, alloy powders, and layer thickness on metal-ceramic bond strength," *J. Prosthet. Dent.*, vol. 119, no. 3, pp. 481–487, 2018.
- [46] L. Slokar, J. Pranjić, and A. Carek, "Metallic materials for use in dentistry," vol. 7, pp. 39–58, 2017.
- [47] F. Engineering, "Comparison of Dental Prostheses Cast and Sintered by SLM from Co-Cr-Mo-W Alloy," vol. 16, no. 4, pp. 201–207, 2016.
- [48] A. Thompson, D. McNally, I. Maskery, and R. K. Leach, "X-ray computed tomography and additive manufacturing in medicine : a review," vol. 17, 2017.
- [49] M. V Swain and J. Xue, "State of the Art of Micro-CT Applications in Dental Research State of the Art of Micro-CT Applications in Dental Research," no. December 2009, 2014.
- [50] M. Borba, U. D. P. Fundo, W. G. M. Jr, and J. Griggs, "Evaluation of the adaptation of zirconia-based fixed partial dentures using micro-CT technology," no. October, pp. 1–8, 2013.
- [51] A. Kakaboura, C. Rahiotis, D. Watts, N. Silikas, and G. Eliades, "3D-marginal adaptation versus setting shrinkage in light-cured microhybrid resin composites," vol. 3, pp. 272–278, 2006.



- [52] K. Ejima *et al.*, “Influence of metal artifacts on in vivo micro-CT for orthodontic mini-implants,” vol. 54, no. 1, pp. 55–59, 2012.
- [53] Y. Choi, J. Koak, S. Heo, S. Kim, J. Ahn, and D. Park, “Comparison of the mechanical properties and microstructures of fractured surface for Co-Cr alloy fabricated by conventional cast , 3-D printing laser-sintered and CAD / CAM milled techniques,” pp. 67–73, 2014.
- [54] J. A. Slotwinski, E. J. Garboczi, P. E. Stutzman, C. F. Ferraris, S. S. Watson, and M. A. Peltz, “Additive Manufacturing,” vol. 119, pp. 460–493, 2014.
- [55] J. P. Kruth, M. Bartscher, S. Carmignato, R. Schmitt, L. De Chiffre, and A. Weckenmann, “CIRP Annals - Manufacturing Technology Computed tomography for dimensional metrology,” *CIRP Ann. - Manuf. Technol.*, vol. 60, no. 2, pp. 821–842, 2011.
- [56] W. W. Wits, S. Carmignato, F. Zanini, and T. H. J. Vaneker, “Porosity testing methods for the quality assessment of selective laser melted parts,” *CIRP Ann. - Manuf. Technol.*, vol. 65, no. 1, pp. 201–204, 2016.
- [57] P. Jyothi, S. Kamishetty, and S. Reddy, “Review article Micro Computed Tomography – Potential Research and Diagnostic Tool in,” vol. 2, no. 3, pp. 43–49.
- [58] a. K. Taslicali and S. Ercan, “Standard Test Methods for Bend Testing of Material for Ductility,” *J. Aeronaut. Sp. Technol.*, vol. 2, no. 4, pp. 55–65, 2006.
- [59] Lava TM Milling Center Starberg Kera Disc (Milled)  
<https://lavazentrum.com/en/products/keradisc>
- [60] ASTM International, “Standard Test Method for Knoop and Vickers Hardness of

- Materials,” *Astm E384-11*, pp. 1–43, 2014.
- [61] “Reinshaw Co28Cr6Mo-LC,” vol. 6, no. 2, p. 103, 1393.
- [62] “IPS InLine System ®.” <https://www.ivoclarvivadent.com/en/p/all/products/metal-ceramics/ips-inline-system/>
- [63] ASTM Standard F1044-05, “Standard Test Method for Shear Testing of Calcium Phosphate Coatings and Metallic,” vol. 05, no. Reapproved 2011, pp. 1–6, 2012.
- [64] N. Kaleli and D. Saraç, “Comparison of porcelain bond strength of different metal frameworks prepared by using conventional and recently introduced fabrication methods,” *J. Prosthet. Dent.*, vol. 118, no. 1, pp. 76–82, 2017.
- [65] X. Han *et al.*, “Comparative analysis of mechanical properties and metal-ceramic bond strength of Co-Cr dental alloy fabricated by different manufacturing processes,” *Materials (Basel)*, vol. 11, no. 10, 2018.
- [66] L. Wu, H. Zhu, X. Gai, and Y. Wang, “Evaluation of the mechanical properties and porcelain bond strength of cobalt-chromium dental alloy fabricated by selective laser melting,” *J. Prosthet. Dent.*, vol. 111, no. 1, pp. 51–55, 2014.
- [67] ISO 9693-1:2012 “International Standard International Standard,”Dentistry-Compatibility testing- Part 1: Metal ceramic systems.
- [68] X. W. Ren, L. Zeng, Z. M. Wei, X. Z. Xin, and B. Wei, “Effects of multiple firings on metal-ceramic bond strength of Co-Cr alloy fabricated by selective laser melting,” *J. Prosthet. Dent.*, vol. 115, no. 1, pp. 109–114, 2016.
- [69] S. Kim, J. Koak, S. Heo, S. Kim, and M. Kim, “Co-Cr alloy copings fabricated with

a selective laser sintering technology,” pp. 337–344, 2015.

- [70] M. Vojdani, K. Torabi, E. Farjood, and A. Khaledi, “Comparison the Marginal and Internal Fit of Metal Copings Cast from Wax Patterns Fabricated by CAD/CAM and Conventional Wax up Techniques.,” *J. Dent. (Shiraz, Iran)*, vol. 14, no. 3, pp. 118–11829, 2013.
- [71] L. Zuskova, N. A. Al Mortadi, R. J. Williams, K. H. Alzoubi, and O. F. Khabour, “Comparison of Overall Fit of Milled and Laser-Sintered CAD/CAM Crown Copings,” *Int. J. Dent.*, vol. 2019, pp. 1–5, 2019.

## Appendices

### **Appendix A: Set-up of Micro-CT Nikon XT 225 ST model**

1. Plug-in and turn on the machine.
2. Login screen enter the password and select run the program.
3. Once you are signed in the inspect-X-software are appeared and two windows will appear as shown on the Appendix (A.1). One for the image view and the other one control view. Image view that have tools to determine the appropriate KV, MA and position of the sample. Control view that shows the auto-condition of the unit as well as the scan area.
4. Position the sample on the Jigs and make sure the handle of the sample is secured and oriented parallel to the beam area.
5. Look at the “Control view” window as shown on the Appendix (A.2): if the systems good and interlocks are set, a green check mark will be visible at the bottom of the window and X-ray indicators will be green. Then set the “x-ray off” as shown on the picture.
6. If the green check mark is an “X” and x-ray indicators is white and set to “no x-ray interlock” that mean the cabinet door is not closed properly or the key interlock is set “off”
7. Check the system status using the (i) (Big blue i) icon if necessary.
8. System setup screen, as shown on the Appendix (A.3):

At “Control View”: after determining the system is ready to go, starter for setup the screen and locate the auto-condition setti

9. Auto-condition setup for the CT scan, as shown on the Appendix (A.4):
  - a. Step 1:
    - i. Ensure no samples have been left on the stage and “Home” the manipulator icon.
    - ii. Click “Ok” when the dialog box appears.
    - iii. Status bar will pop up during the home process. The status bar will tell you when the homing has completed.
  - b. Step 2:
    - i. Use default setting (do not change max KV, should be at 225)
    - ii. Select auto-condition
    - iii. X-ray control area will change from green “x-ray off” box to a red “auto-condition” that mean x-ray are now on and the unit is auto-conditioning. Let the auto-condition start and leave it for 5 minutes to reach the maximum KV then select the “stop” bottom.
10. Running a CT scan:
  - a. Step 1, as shown on the Appendix (A.5):
    - i. Select CT tab, then the window will show the image of the sample.
    - ii. Make sure the sample is secure and centered on the stage.
    - iii. Select “new sample” then the next window will be appearing on the tab list.

b. Step 2:

- i. From the information bar: a box will appear and requesting a Data base name. then naming your data set in the location shown at the picture, as shown on the Appendix (A.6).

Once the file name, click on the nest tab called “position + optimize “

c. Step 3:

- i. From the “position and optimize “icon, that helps to set the parameters of the three-unit-bridge samples for the CT scan image.
- ii. Switch the x-ray on, as shown on the Appendix (A.7)
- iii. Adjust the manipulator position: unlocked all the tilt plane (Y and X) to let the manipulators stage moved up and down and press save for this setting.
- iv. Voxel size choose at (15 micron) resolutions, geometric magnification at (13.332) and magnification at (80).
- v. Adjust the parameters for the image CT scan:
  - a. Beam energy for KV= 220
  - b. Beam current for MA= 50
  - c. Power for W= 11
  - d. Histogram value should always between the 10000 to 65000.

d. Step 4:

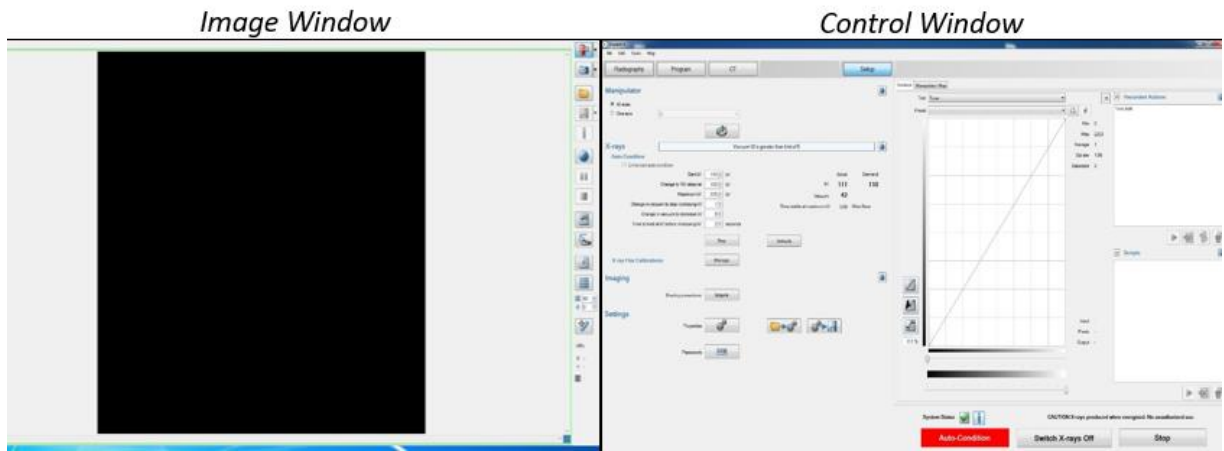
- i. From the “correction”, move the sample out of the view them enter your current (50 uA) and the energy (220 KV), then select “New”

shading correction or updating the old correction with the same setting using the drop-down tab and then press “update” option, as shown on the Appendix (A.8).

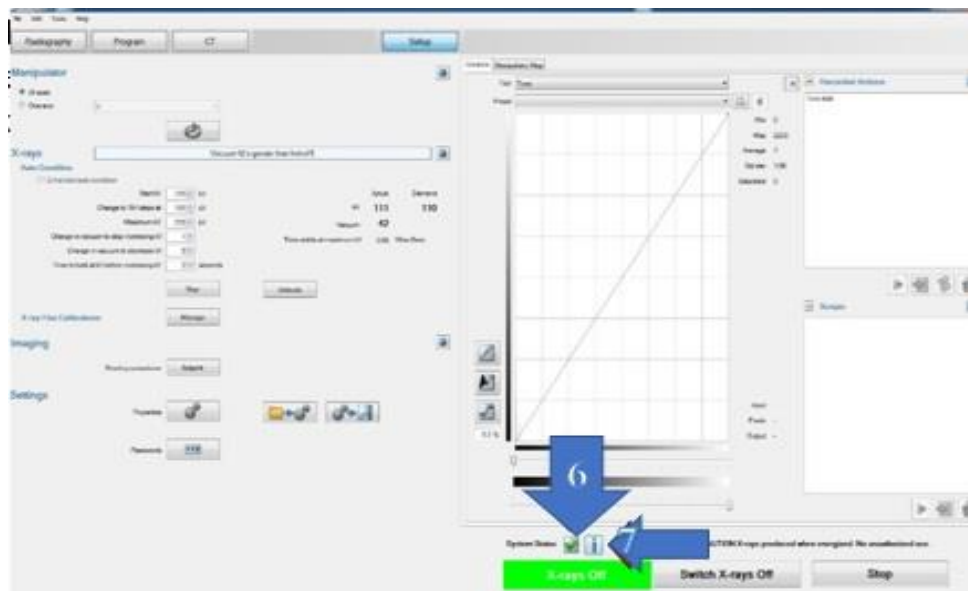
- ii. Image window should appear as below, with the object out of the view prior to shading correction. A dialog box will appear where you select the filtration which is Copper size (1 mm) then press “generate” the two-dialog option will appear on the screen to reminding you to move your object and check the filter if it there, as shown on the Appendix (A.9).
- iii. Once the shading correction is completed, then select the “Acquired data set”

e. Step 5:

- i. From the “Acquired data set”, this tab where you can find the option to “Minimize ring artifact” to the (4), that indicates the four direction, followed with optimization Number of the projection (1570) half projection, and number of frames to average (3).
- ii. The estimation of the scanning time is provided (26) minutes
- iii. Select the computer that will process the image for the reconstructions stage that want to acquire the data set to “Drop-down new” then press “acquire” option, as shown on the Appendix (A.10).
- iv. Then press the play bottom to run the CT machine.
- v. Notes: this steps and parameters can be used for the multiple CT scans and no need to change any of them.

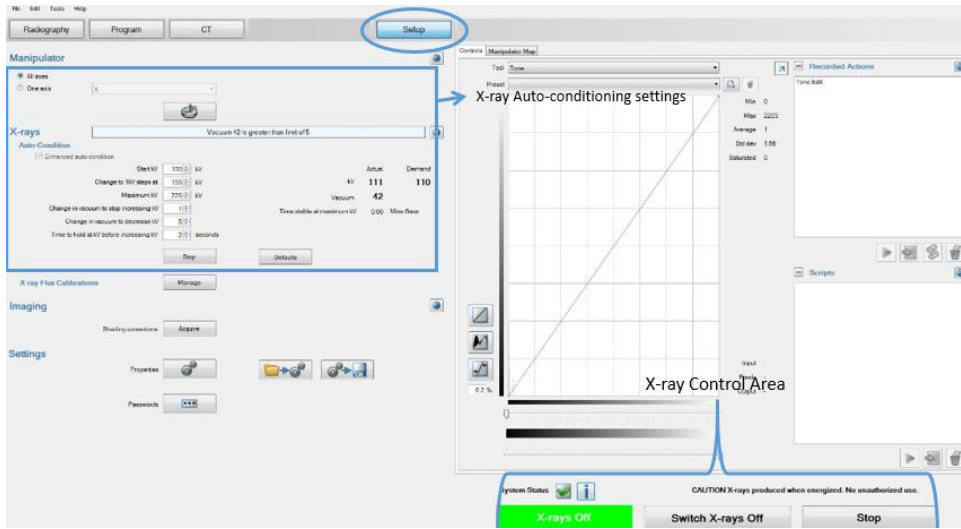


**Appendix A-1: Windows view for the image of micro-CT and Control view display.**

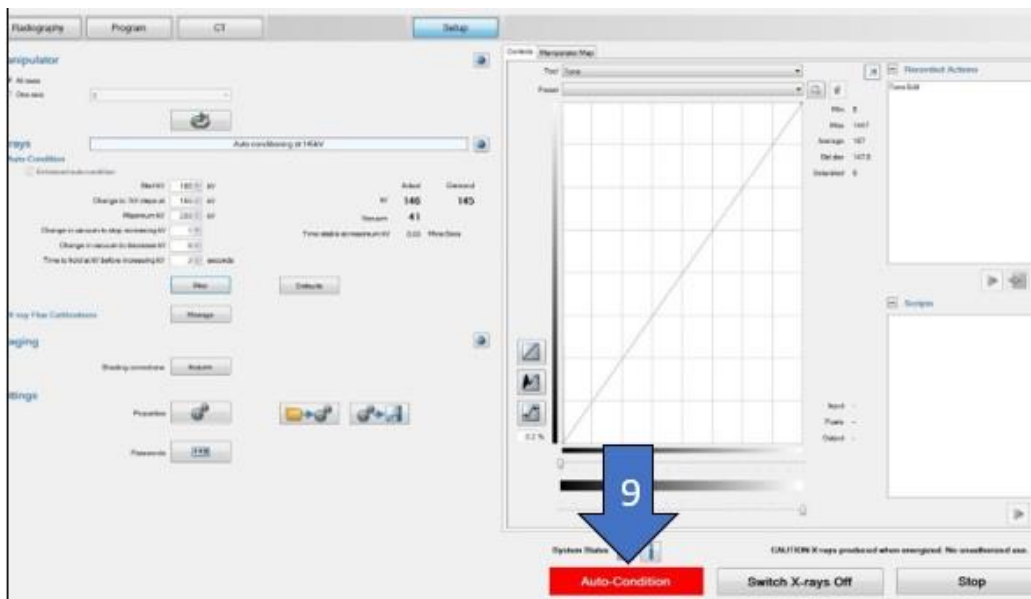


**Appendix A-2: Control view commands bar and view display.**

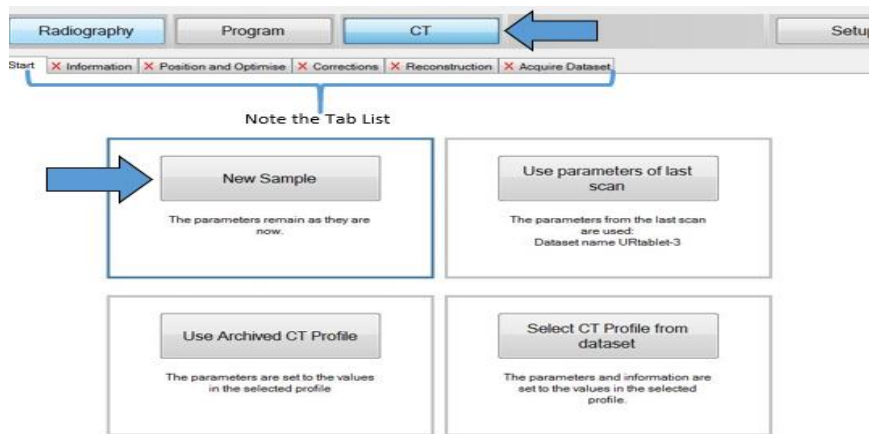




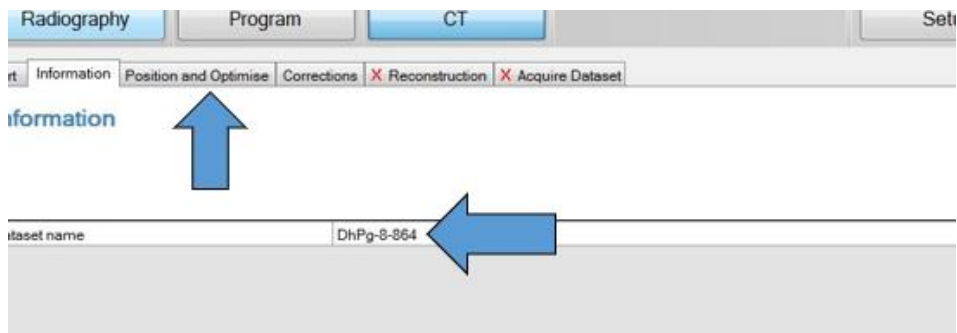
Appendix A-3: Control view setup screen.



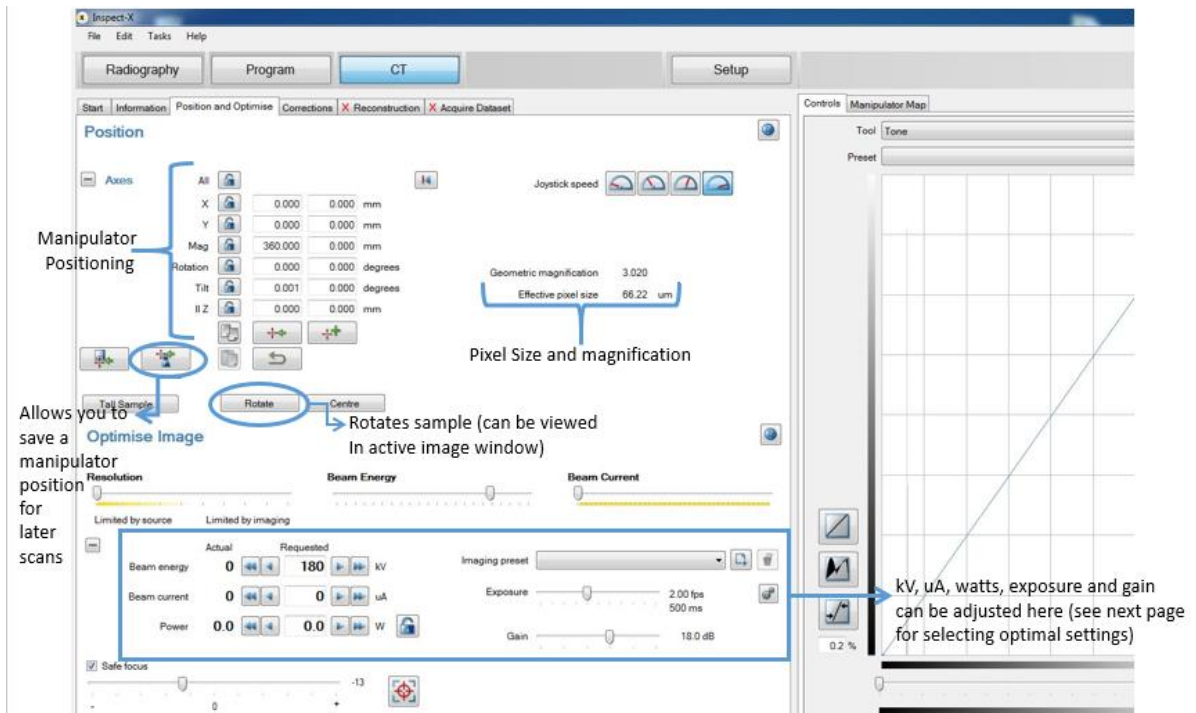
Appendix A-4: Auto-conditioning the CT.



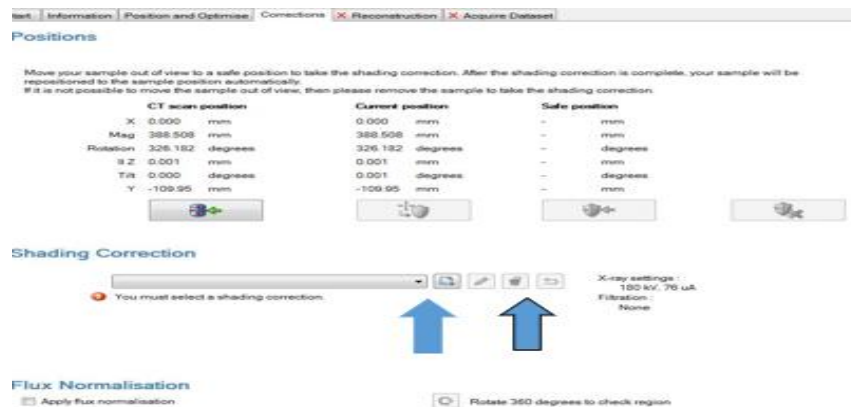
**Appendix A-5: How to select the CT and running the machine.**



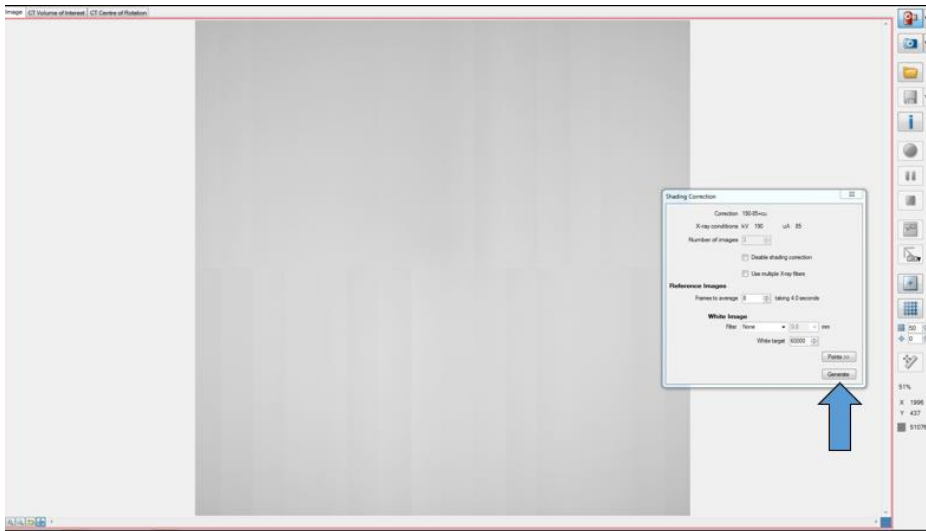
**Appendix A-6: Select the data base name and run the position and optimize bar.**



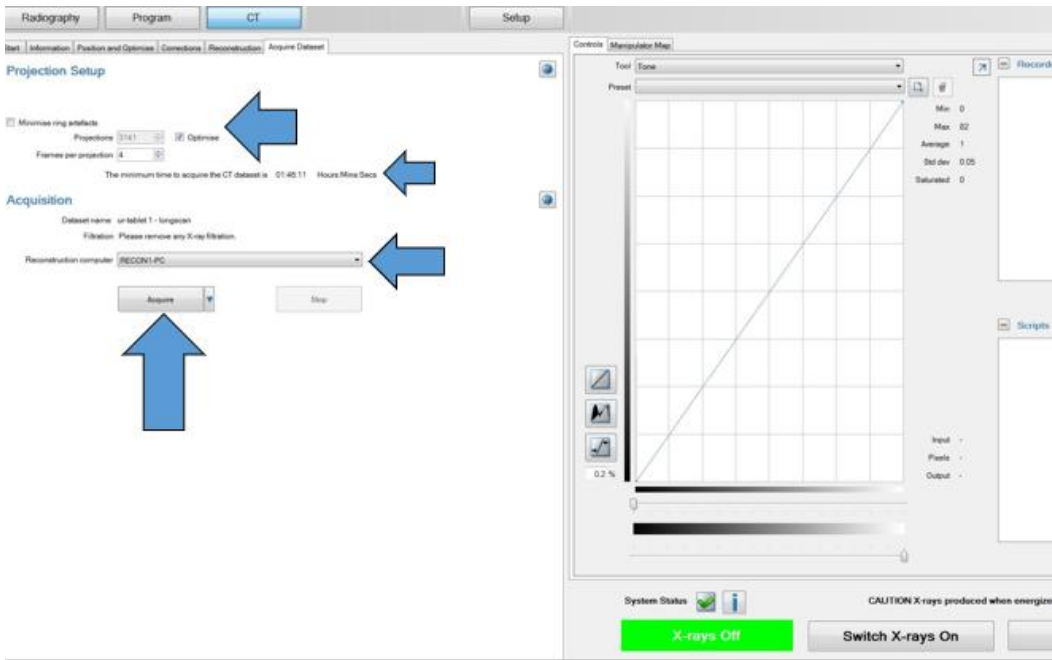
**Appendix A-7: Parameters setup for the CT-image.**



**Appendix A-8: Correction shade setup.**



**Appendix A-9: Image view window display.**



**Appendix A-10: Acquired data set and CT-run.**

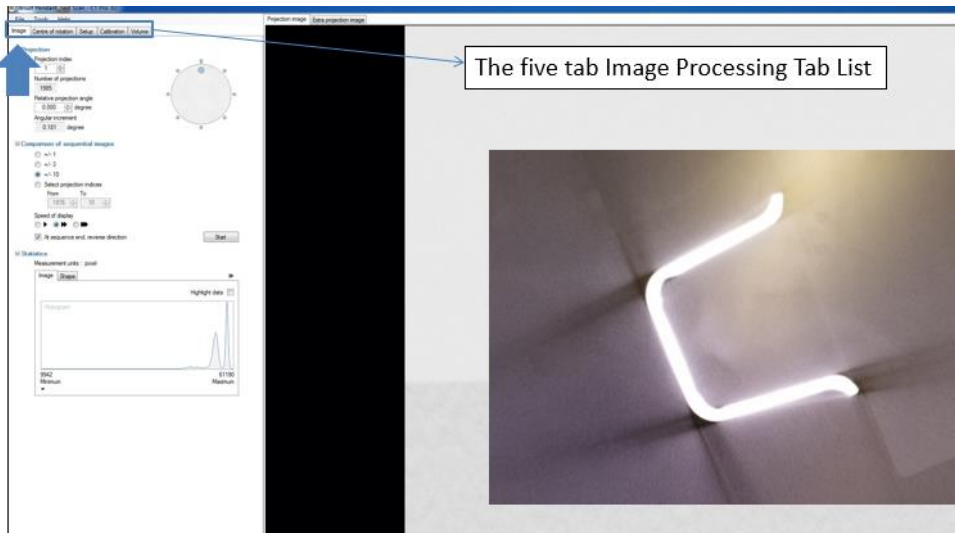
## Appendix B: 3D-Pro program setup for CT-reconstruction

1. Select the file → open
2. Locate the file you want to open
3. Double left clicks on the file to launch the processing sequencing
4. Once the file is open you will be brought you to the first step in the image processing sequence, as shown on the Appendix (B.1)
5. Image tab 1: check the projection image and extra projection image couple time → to make sure if there is any significant different in the object while its movements occurred during the CT scan image.
6. Center of rotation tab: if the object had a minimal movement during the scan acquisition, then proceed to the “center of rotation”
7. Select the slice from “accuracy” tab by choosing “standard”, then under the slice selection choose “Dual” then press start, when the center of rotation is completed, the upper and lower pixel are changed and will be marked as found. Then repeat the same step for the “high quality” under the “accuracy” tab. Press start, when the center of rotation is complete, the upper and lower pixels will be marked as found too, as shown on the Appendix (B.2).
8. Beam Hardening Correction:
  - When the center of rotation has been found, proceed to set up tab.
  - See the red line doesn't go through of the material in different density.
  - Position of the line across the object
  - Then check the re-constructed are present.
  - Then select start, that will take several minutes to complete the process.

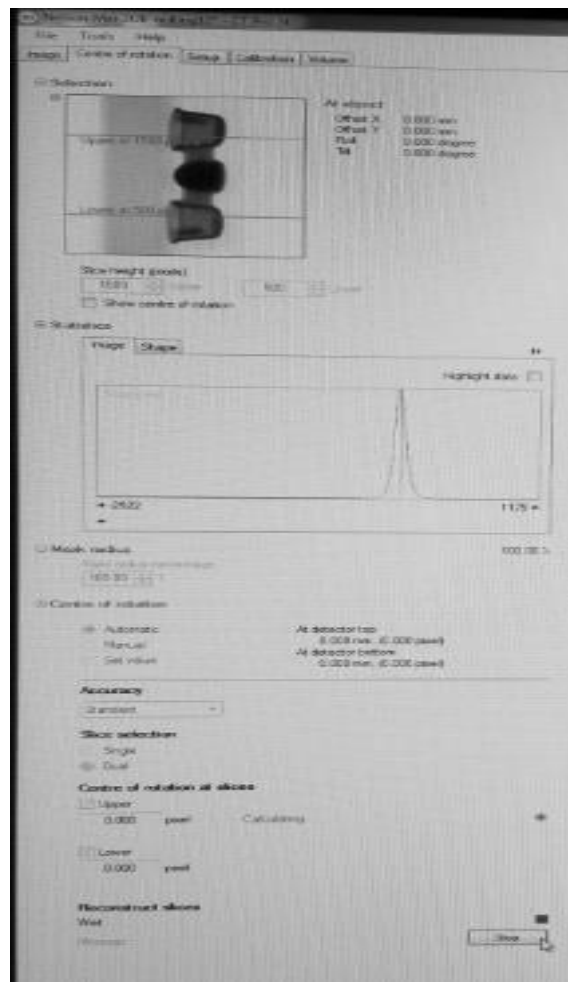
- The histogram shows, the line drawn across the object, then the line cross to it as shown on the figure as cupping characteristics of beam hardening. When it shows “flat peaks” or near to it. Once the all the 6 percent on the histogram are good, followed to the corresponding to the best projection. Usually the percent 1, 2 or 3 proceed to the “volume tab”, as shown on the Appendix (B.3)

9. Volume tab:

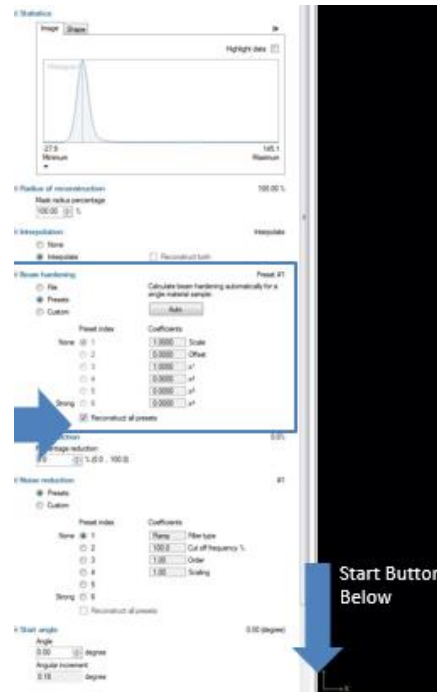
- Select and shrink the region of interest (ROI) for volume re-construction by moving the red (ROI) around the object of interest.
- Select the output of the format, then click “start” to proceed immediately.
- Then saved all the file on the VGL then exported to the other program VG. Studio.



Appendix B-1: The image tab processing.



Appendix B-2: Center of Rotation Setup.



**Appendix B-3: Beam Hardening setup.**



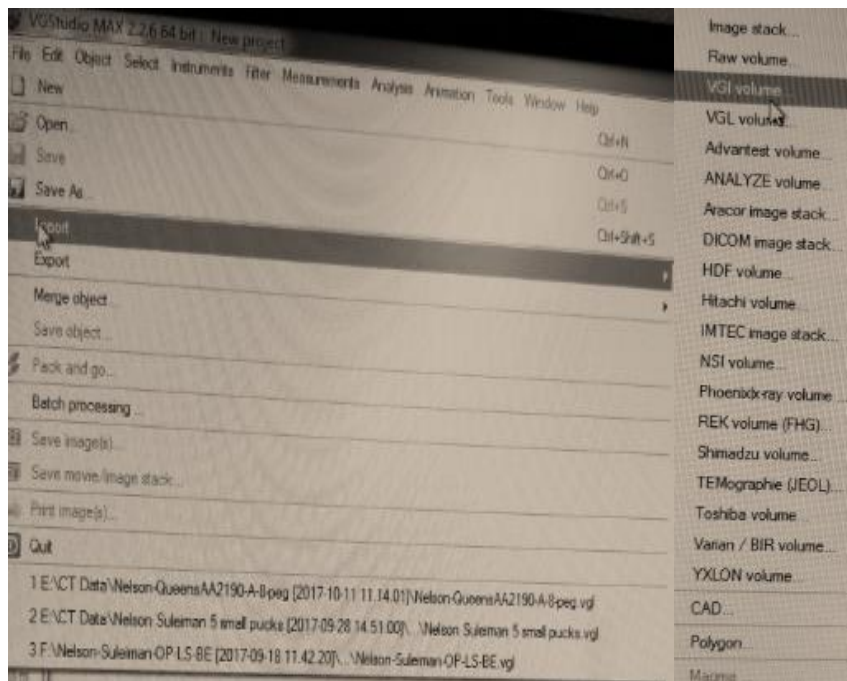
### **Appendix C: GG Studio Max Tools setup**

1. Open the file on VG studio from drop-down option
2. Import-→from the 2<sup>nd</sup> set of the drop-down options select “VGi volume”
3. VGi volume file selected dialog box will appear, as shown on the Appendix (C.1)
4. Select browse to locate the volume file you want to use
5. locate and select the desired volume file from saved location on the computer or external hard drive
6. once the file selected, then return to the VGi volume file selected dialog, as shown on the Appendix (C.2).The file name will appear, then select “next” from the option provided at the bottom of the dialog box.
7. after the “next” option the new set it will shows then select “import” option
8. the dialog box provides the “load as” options, that’s allow the VG studio to handle the volume file and changing the size and type of the file, as shown on the Appendix C.3
9. to change the file size and type. Select the “load as” tools, the new tab will show and changed from the “32 in bite” to “16 un sight”, as shown on the Appendix (C.3).
10. Then from the Histogram bar bottoms to view the grey scale that represents the acquired volume. Then minimized the window and start reducing the maximum and minimum grey scale values of the histogram.

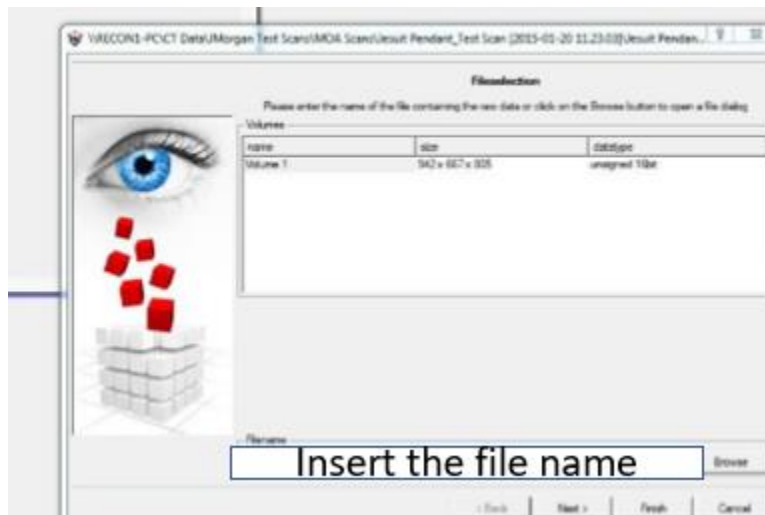
11. Scroll the mouse over the redline along the right border of the histogram and move it close to the edge of the histogram peak to the right side, as shown on the Appendix (C.4)

12. Once the histogram grey scale is defined, then refer to the “load as” dialog box and click “finish” then the project will now begin import. Make file and name related to the “16-bite”, as shown on the Appendix (C.3).

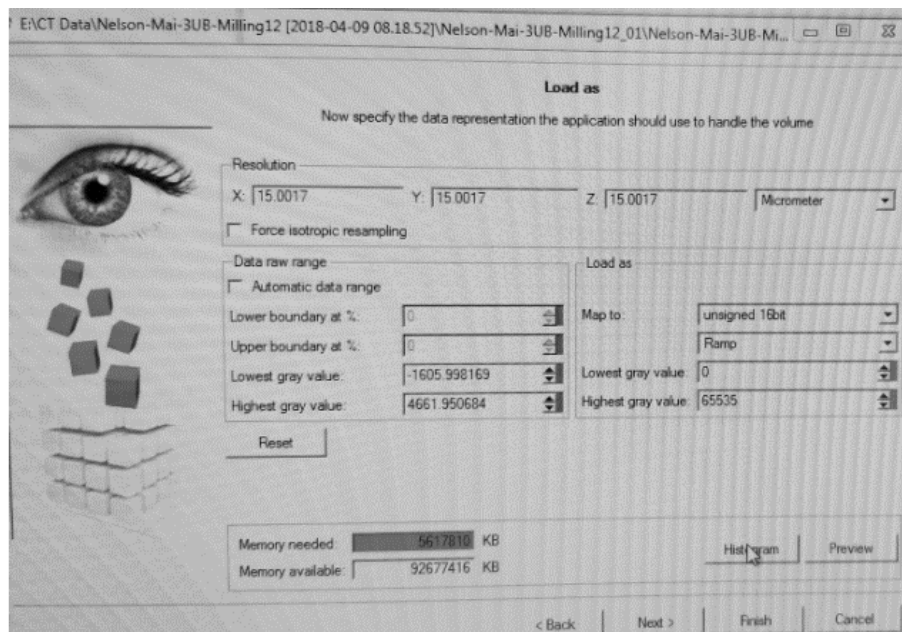
13. Then hit back for the file and choose export file and should be under the 16-bite, then choose file type is “tiff” (.tif) and save the file follow this type of the file.



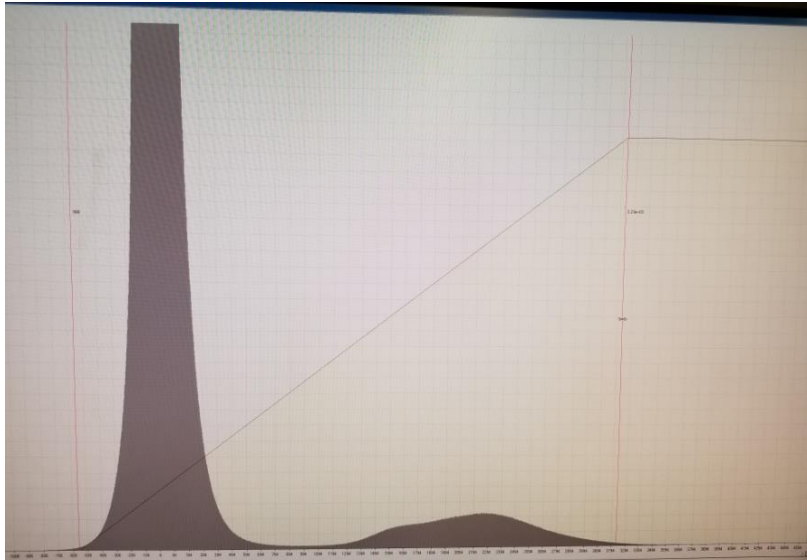
### Appendix C-1: Opening/Importing a Volume File.



**Appendix C-2: Select the file volume.**



**Appendix C-3: Changing the file size and volume under the Load file.**



**Appendix C-2: The histogram grey scale border.**

## Appendix D: Analysis of the Geometric Surface Deviation

After the scanning protocol is complete, the image obtained from the micro-CT scanner is reconstructed previously for the porosity analysis into (.vff) files to be presented as a 3D volume object. This construction done by the Micro-View 3D Image Viewer and Analysis Tools (Parallax Innovation, Ilderton, ON). Once the files are constructed, they are converted to surface files (.stl) within the micro-view, to be exported to, and analyzed with Geomagic ® Qualify (Geomagic, Morrisville, NC). All the series of steps used for the analysis of the micro-CT data files, from the conversion of the re-constructed images (.vff) into surfaces (.stl) to the analysis tools used within Geomagic ® Qualify described below.

Step 1: Conversion of (.vff) to (.stl) in Micro-view:

- I. Open the(.vff) image file. The file within Micro-view, File → open → select file. The file should contain a series of image slices which make up the volume of the imaged object. By placing the mouse pointer rolled over the image volume and left clicking while dragging the mouse, the orientation of the image volume can be selected and manipulated.
- II. Within the Micro-view program, the “Tool and Application” tab should be in the left side of the window. Press on the “Standard ROI” icon under the tool and application tab. That will provide a yellow region of interest (ROI) box in the image volume of the right.
- III. Within the standard ROI tab, the “Box” tool and “Millimeter” unit is set as the default options. These defaults setting may remain the same or it vary from object to other.

- IV. The select the region of interest from which the surface files will be created, place the mouse and rolled over each of the walls of the yellow ROI box, and click on the mouse wheel to extend these walls in the horizontal and vertical directions over desired region. This is well causing a change in the ROI size and center of (X, Y, Z) coordinates, that shown on the tab located on the left of the program window. The “ROI size” and “ROI center” coordinates can be changed to make fine adjustments to the region of interests.
- V. Once the desired “ROI” is shown within the yellow ROI box, choose the “Visualize” tab on the tool bar located at the top of the program window, and choose the “Iso-surface” option.
- VI. Under the “Iso-surface properties” of the “Iso-surface” tab fill the desired image threshold value (Note: for each sample threshold were selected through the histogram grey scale of the image CT by choose the margin area of the three-unit bridge and make a line crossing over the air and metal (the line should be equal on each side) then take the median of the high and low threshold and divided by 2 to give an average of the threshold for each sample). That required for certain of the iso-surface. Adjust the surface quality factor to (75%) and click the “update” icon. This will create the desired surface from the image ROI on the right. Once the surface is deemed suitable, select the “Save Surface” option, and save the resultant iso-surface as a (.stl) file to the desired location, as shown on the Appendix (D.1)

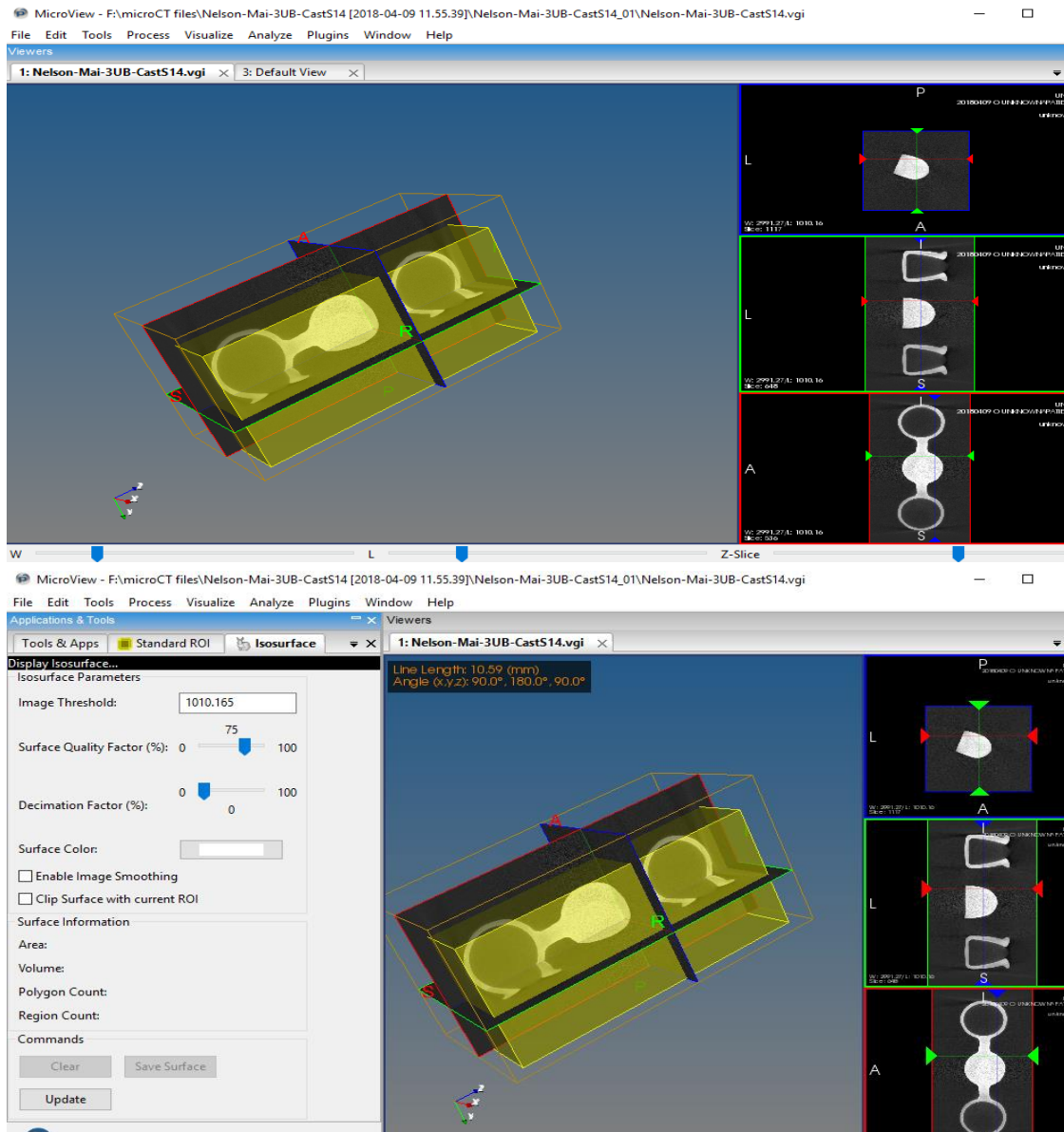
Step 2: Analysis of Surface Deviation between the original 3D virtual (3UB) model and the (3UB) dental manufactured from 3D-printing, milled and casted.

- I. Open the (.stl) containing the iso-surface of the (3UB) dental manufactured model. File → open → select file
- II. The file should appear within the “Model Manager” tab to the left of the program window. Right click on the select the option “Set as Reference” this will show as “REF-“appearing adjacent to the file name in the Model Manager window.
- III. Import the (.stl) containing the iso-surface of the original 3D virtual (3UB) model: File → Import → Select file
- IV. Right click the imported file in the (Model Manager) tab and select the option “Set as Test” appearing adjacent to the file name in the (Model Manager) window.
- V. Select the “Rectangular Icon” the 6<sup>th</sup> icon from the top located on the vertical toolbar at the right of the program window. Use this option to highlight the rectangular faces of the three-unit bridge by outlining the edges of the faces within the rectangular cursor.
- VI. Once all faces of the three-unit bridge are highlighted for “REF- “and “TEST-“surfaces, click on the “Home” tab located at the top of the program window, and select “Best Fit” option. By applying the best fit alignments tool, all surfaces of the three-unit bridge will be registered.
- VII. To compare the surface deviation between the 3UB dental manufactured sample and original 3D virtual 3UB model iso-surface, click on the “Home” tab at the top of the program window, and select the “3D compares”. This

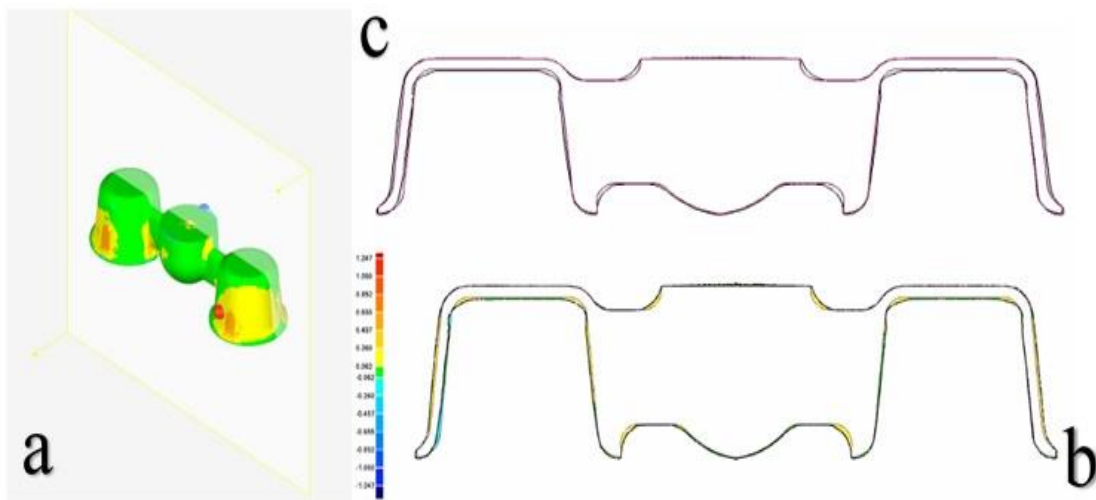
will create a 3D-color plot comparing the deviation in the References and Test surfaces, as shown on the Appendix (D.2a)

- VIII. The cross section through the iso-surface, along the (X, Y, Z) planes could also be compared, to determine the change in surface deviation through each section. On the “Home” tab click the “Section Through Object” to select the plane along the which analysis is desired. For the compare on the 3UB dental manufacture model deviation through the three-plane direction (X-Y), (X-Z), and (Y-Z) plane, as shown on the Appendix (D.2b)
- IX. To analysis the section through the object select “2D dimension” from “Home” tab at the top of the program window, as shown on the Appendix (D.2c). This tool allows the user to select various locations along the references (3UB dental manufacture model) profiles to determine the vertical and horizontal deviation of the test (original 3D virtual 3UB model) surface relative to the references surface at the (X-Y) plane. Followed with the cross section of the object at the (X-Z) plane and the center of the model at (Y-Z) plane.
- X. To determine the point from the left tab window, it will be a mode between two point of the “REF- “and “TEST-“then selected different point and analysis it.
- XI. After finishing all the three sectional planes comparing and analysis, then the report it will be generated for the 3D and 2D comparison.





**Appendix D-1: ROI and the Iso-surface properties.**



**Appendix D-2: (a) 3D color plot, (b) Comparison between the reference and test, (c) 2D comparison**

## **Appendix E: Metallurgical Analysis setup using the Nikon Digital Eclipse Camera DXM 1200 & Nikon ACT-1, Version 2-20**

- I. Starting the ACT-1 from the Start menu:
  1. First, check that the camera is properly connected to the PC. Then, turn ON the power to PC. Click on the Start button at the lower corner of the screen. The Start menu appears.
  2. Click on Programs and select ACT-1 from the Programs List.
  3. The ACT-1 window will open.
- II. Capturing Images:
  1. Click on the Image on the command bar. Then select the scale and magnification you want to use for the Live image (10x) Yellow lens.
  2. Then, hit the Exposure button.
  3. ACT-1 In Exposure Operation dialog box appears during image capture. Click on the STOP button if you wish to stop image capture.
- III. Saving and Loading the setting file:
  1. File menu command list: Click on File in the menu bar. Then, select Setting/Save in the File menu command list. The Save Setting File dialog box appears.
  2. Save Setting File dialog box: choose where to save the setting file. Click on the down arrow button at the right side of the Save in box and select a location from the drop-down list. Next, type in a setting filename as “JPG” file style. Then, click on the Save button.
- IV. Loading a setting file:

1. File menu command list: Click on File in the menu bar. Then, select Setting/Load in the File in the File menu command list. The Load Setting File dialog box appears.
2. Load Setting File dialog box: Select where the setting file has been created and saved. Click on the down-arrow button at the right side of the Look in box and select the location from the drop-down list. Select the target setting file. Click on the Open button.

## Curriculum Vitae

**Name:** Mai EL Najjar

**Post-secondary** Ajman University of Science and Technology

**Education and** Ajman, United Arab Emirates

**Degrees:** 2003-2009 DDS

Fanshaw College

London, Ontario, Canada

Sept – Dec 2013 ESL GAP 5

The University of Western Ontario

London, Ontario, Canada

2016-2019 MEd.

University of British Columbia

Vancouver, British Columbia, Canada

2019-present MSc. of Prosthodontics

**Honors and** Recognition of services with sincere appreciation for the pre-

**Awards:** clinical dental education from the Dean of the Schulich of

Medicine and Dentistry, Faculty of Dentistry

The University of Western Ontario

November 2014

Third Place Poster Presentation Award “Advanced 3D Metal

Additive Manufacturing for Dental Substructures”

during the 13th CAD/CAM & Digital Dentistry Conference, Dubai,

UAE.

May 4-5<sup>th</sup>, 2018

**Related Work**

Adjunct Clinical Professor- Simulation Clinic

**Experience**

Schulich of Medicine and Dentistry, Faculty of Dentistry

The University of Western Ontario,

2012-2019

Teaching Assistant

The University of Western Ontario

2018-2019

**Publications:**

Mai EL-Najjar, Yara Hosein, Amin S. Rizkalla “Advanced 3D Metal Additive Manufactures for Dental Substructures”, *Dental Tribune*, published in Dubai, UAE, July-August 2018, No. 4, Vol. 8 page 36.

M. Jacinta M.C. Santos, Heleine Maria Chagas Rêgo, Anuradha Mukhopadhyay, Mai El Najjar, Gildo C. Santos, “Effect of artificial aging on the surface roughness and microhardness of resin-based materials”, Jr. *Gen Dent*, 2016 Mar/Apr; 64(2): e13-e17.